In presenting this thesis in partial fulfillment of the requirements for an advanced degree at Idaho State University, I, Dallin James Steele, agree that the Eli M. Oboler Library shall make it freely available for inspection. Further, I state that permission for extensive copying of this thesis for any scholarly purposes may be granted by the Dean of the Graduate School, or by the Dean of the College of Engineering, or by the University Librarian. It is understood that any copying for publication of this thesis for financial gain shall not be allowed without my written permission.

Signature: _____

Date: _____

A Flexible System for Interrogating the Out-of-Plane Emissions from 2D Photonic Crystals

by

Dallin James Steele

A thesis submitted in partial fulfillment of the requirements for the degree of

MASTER OF SCIENCE

in

NUCLEAR SCIENCE AND ENGINEERING

Idaho State University

2015

To the Graduate Faculty:

The members of the Committee appointed to examine the thesis of DALLIN JAMES STEELE find it satisfactory and recommend that it be accepted.

_____

Eric Burgett

Major Advisor

_____

Tony Hill

Committee Member

_____

David V. Beard

Graduate Faculty Representative

Table of Contents

List of Figures vi
Abstract ix
Introduction 1
Background 3
Current Sensor Technology 3
Light Gauge 3
Photonic Crystal Fabrication 5
Interrogating Crystal Off Axis 7
Theory 9
Photonic Crystal Basics 9
2D Crystals 10
3D Crystals 12
Methodology 14
Hypothetical World 14
Ideal Setup 14
Assumptions for Real World Application 15
Design Considerations 16
Collection Point of the Emission Response from the Crystal 16
Experiment Coordinate System Definition 17
Eucentric Design 18
Order of Stages 19
Stand Design 21
Modification of an XRD stand 21
Bottom Rotation Table 22
Sample Arm 24
Rotation Arm for Collection Fiber 27
Optical Viewing Piece 33
Original Setup 34
Final Setup 35
Calibration of Spectrometer 36
Background and Source Measurements 36
Fiber Alignment Tool for Spectrometer 38

Repeatability of Measurements 40
Wavelength Calibration 42
Combining Multiple Windows 43
Experimental Procedure 47
Analysis and Results 50
Initial Results 50
Crystal Response / Light Source Spectrum 51
Smoothing 51
Crystal Response / Light Source Spectrum 55
Remove Scaling 56
Crystal Response / Reflection of Light Source on Steel 59
Light Source / Reflection of Light Source on Steel 59
Crystal Response of the Initial Test / Reflection of Light Source on Steel 60
Crystal Response of the Full Test / Reflection of Light Source on Steel 63
Color Analysis 67
Purpose of Color Plot 67
CIE 1931 Color Matching Function 67
Converting the Spectrum to sRGB Values 68
Color Plot 69
Summary 70
Works Cited 72

List of Figures

Figure 1: Potential LightGauge sensor placement in relation to grain structures of a given material [1] 4

Figure 2: Dual beam FIB which was used to produce the photonic crystal used in project [5] 6

Figure 3: Images of the photonic crystal used for this project [1] 7

Figure 4: 1D, 2D and 3D photonic crystals [6] 9

Figure 5: 1D Photonic crystal also known as multilayer film [6] 10

Figure 6: 2D crystal lattices: square, triangular and honeycomb lattices 11

Figure 7: Triangular lattice of a 2D photonic crystal [6] 12

Figure 8: Diagram of assumptions 15

Figure 9: Coordinate system definition 17

Figure 10: Eucentric height 18

Figure 11: Multiple stages 20

Figure 12: Example 2 of why stage ordering matters 20

Figure 13: Bottom rotation table 22

Figure 14: Arm extended from bottom rotation table 23

Figure 15: Sample rotation table 24

Figure 16: Z movement 25

Figure 17: Sample arm with the rotation and position stages for the sample 26

Figure 18: Fiber rotation arm which rotates the collection fiber around the crystal at a fixed distance from the crystal. 27

Figure 19: Base plate drawing. The base plate provides an elevated surface for the fiber rotation table to attach to and aligns the axes of the fiber rotation table and the bottom rotation table to be collinear 28

Figure 20: Drawing of bottom connection arm that attaches to the fiber rotation table. The arm allows the fiber to rotate about the axis of rotation of the fiber rotation table from a distance. 30

Figure 21: Drawing of bracket used to attach the two translation stages on the X and Y axes 31

Figure 22: Fiber connector plate used to hold the fiber in place 32

Figure 23: Viewing optic of the XRD stand 33

Figure 24: Original experimental setup using a fiber optic cannula as the collection fiber and the light source sent through the viewing optical piece of the stand 34

Figure 25: Final experimental setup using a reflection probe for a collinear light source and collection fiber 35

Figure 26: Effect of room lights on and off 36

Figure 27: The first and tenth measurement of a light source 37
Figure 28: Light source spectrum measured as the spectrometer window is moved 38
Figure 29: Light source spectrum measured as the spectrometer window is moved after using the fiber alignment tool 39
Figure 30: A Peak of the helium spectrum as the spectrometer window is moved incrementally by 10 nm. 40
Figure 31: Repeatability test of helium spectrum lines by moving the spectrometer window between being centered at 530 and 610 nm repeatedly 41
Figure 32: Calibration Curve for the spectrometer window centered at 535 nm 42
Figure 33: Crystal response as theta is varied using a single spectrometer window 43
Figure 34: A set of three overlapping spectrometer measurement windows measuring the crystal response were taken and then combined. The before and after results are shown 44
Figure 35: The spectra of the crystal response as theta is varied using three measurement windows combined together 46
Figure 36: Initial test using the final test stand setup and only varying theta 50
Figure 37: Light source used to produce the crystal response 51
Figure 38: The spectrum of the crystal response at theta of 50 degrees divided by the spectrum of the light source 52
Figure 39: Smoothed and raw data of the crystal response at theta of 50 degrees 53
Figure 40: The crystal response at theta of 50 degrees divided by the light Source after smoothing 54
Figure 41: Spectra of the crystal response from the entire initial test divided by the spectrum of the light source after smoothing 55
Figure 42: Spectrum of crystal response at theta of 45 degrees divided by the spectrum of the light source without scaling and combining of the spectrometer measurement windows 56
Figure 43: Spectrum of crystal response at theta of 35 degrees divided by the spectrum of the light source without scaling and combining of the spectrometer measurement windows 57
Figure 44: Spectrum of crystal response at theta of 30 degrees divided by the spectrum of the light source without scaling and combining of the spectrometer measurement windows 58
Figure 45: Spectrum of the light source divided by the reflection of the light source on the surface of steel 59
Figure 46: Shows the spectra of the reflected light source spectrum from sample 1 location 2 before and after the normalization with the spectra they are normalized to 60
Figure 47: The normalized spectra of the light source reflection on steel at all 7 locations on 2 samples and their average for the center measurement window 61
Figure 48: Crystal response at each sampling location is divided by the reflection of the light source on steel 62
Figure 49: Final test at phi of 0 degrees while theta is varied 63

Figure 50: Final test at theta of 50 degrees while phi is varied 64
Figure 51: Final test at theta of 40 degrees while phi is varied 65
Figure 52: Final test at theta of 30 degrees while phi is varied 66
Figure 53: CIE 1931 color matching functions. This plot was created using color matching function values found in Wyszeck and Stiles' *Color Science* [15] 67
Figure 54: Color plot of the crystal response. Each square represents a sampling location specified by theta and phi 69

Abstract

A custom test stand was designed and built to interrogate the emission response of a two-dimensional crystal off axis. Previous simulations and experimentation for two-dimensional crystals have been completed mainly within the plane that the crystal is periodic. For the light gauge application, this periodic plane is not accessible to the light source or detector. The spectrum of the crystal response was sampled around the crystal at a fixed distance using the stand and converted to a color plot for quickly identifying patterns.

Introduction

LightGauge is a system that has the potential to increase the safety of nuclear reactors by improving monitoring and increasing the knowledge of fuel changes for modeling and simulation. At the core of the LightGauge system is a photonic crystal which is an engineered structure of periodic material that can be written on many different types of structures of interest. Photonic crystals can be used to control the optical flow of light to prohibit or promote bands at certain frequencies or wavelengths, called band gaps.

The photonic crystals used for this project are two-dimensional, meaning that they are periodic on two axes. Previous simulations and experimentation for two-dimensional crystals have been completed mainly within the plane that the crystal is periodic. For the LightGauge application, the periodic plane is not accessible to the light source and detector. Understanding and measuring the out-of-plane emission response of a two-dimensional crystal is key to the success of the LightGauge system.

This document describes a flexible system for interrogating the out-of-plane emissions from 2D photonic crystals that was accomplished by designing and building a custom test stand. This test stand enables the spectrum of the photonic crystal response to be sampled in the space surrounding the crystal from a fixed distance. The point of collection for the emission response and the light source are collinear by using a fiber bundle. The position of the fiber bundle relative to the crystal can be varied by rotation on two axes.

After the custom test stand had been built, its use was then demonstrated. The calibration of the spectrometer was performed first which was used to measure the spectra of the emission response from the photonic crystal. A series of measurements of the emission response spectra was then completed. The emission response was assumed to be symmetrical and, therefore, all possible locations were not sampled.

The spectra of the emission response from the crystal were then analyzed and used to create a color plot. The light source and coloration from the substrate of the photonic crystal affected the spectra of the crystal's response. These effects were removed during the analysis. The spectra were then weighted by a color matching function and converted to sRGB values for plotting. The purpose of the color plot is to allow for a quick visual synopsis of the crystal response at each sample location. Points of interest can then be further investigated by looking directly at the spectra of the crystal response at those locations.

Background

Current Sensor Technology

A nuclear reactor is a harsh environment for in-situ fuel monitoring, making traditional sensors unfeasible because of its high temperature, high radiation and potential for high pressures. Despite these difficulties, there are a number of specialized sensors used to monitor secondary characteristics of a reactor. The inlet and outlet temperatures of the coolant are measured using thermocouples, and the flux of the reactor can be measured with fission chambers or flux wires. [1] [2]

Light Gauge

The LightGauge system has the ability to function in high radiation environments, providing stress and strain data. The sensor can be placed directly on various reactor components including the fuel pellet and cladding. Not only do these advantages allow for better monitoring of nuclear reactors, but will also allow for increased knowledge of fuel changes for modeling and simulation. LightGauge will also be able to monitor grain boundary changes, the creation of new grain, and expansion of voids. Figure 1 shows potential sensor placement in relation to grain structures of a given material. LightGauge functions in real time which will help to increase the understanding of fuel changes early in the fuel cycle.

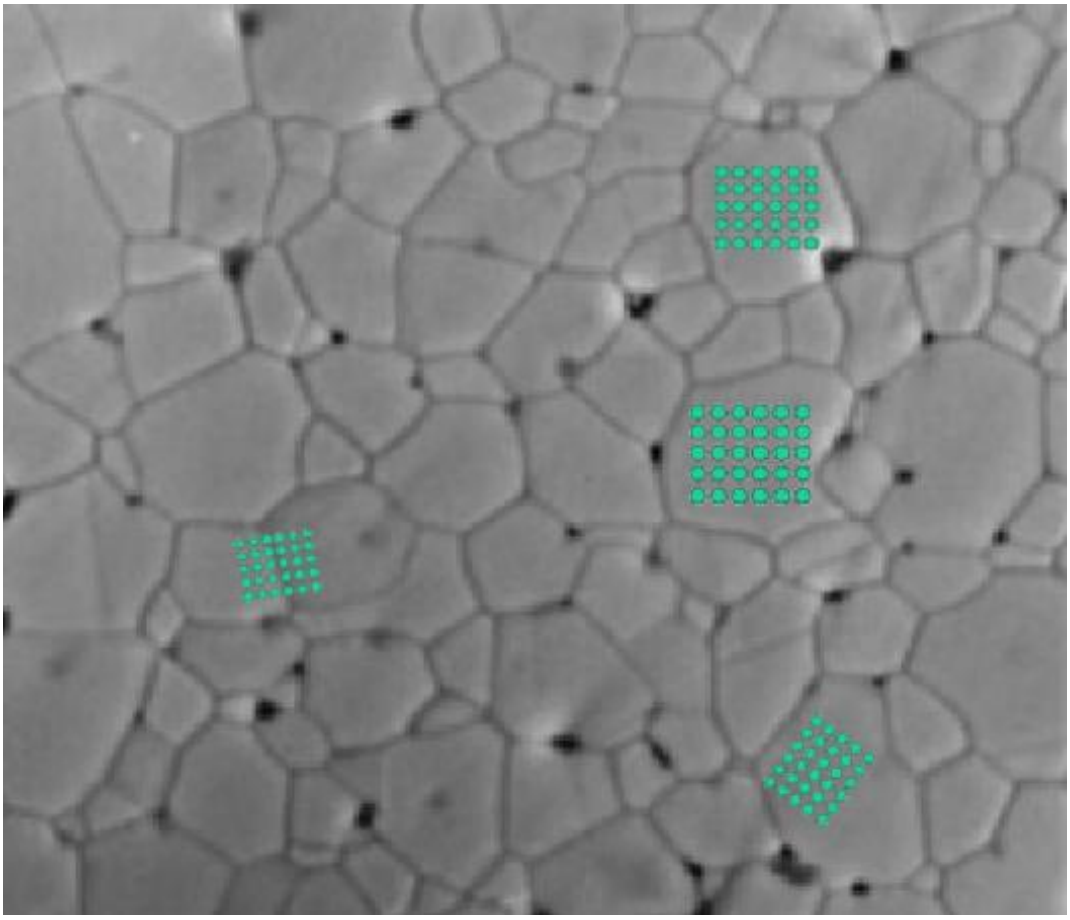

Figure 1: Potential LightGauge sensor placement in relation to grain structures of a given material [1]

Materials in a nuclear reactor environment endure intense radiation, creating damage that is particularly hard on electronics. The LightGauge sensor will be radiation hardened and does not require electronics to be located inside the reactor. The system uses fiber optic cables to both supply light to the sensor and sends back its return signal, enabling the electronics of the system be kept outside of the reactor.

At the core of the LightGauge system is a photonic crystal. The crystal controls the optical flow of light by prohibiting or promoting bands at certain frequencies or wavelengths called band gaps [3]. The wavelength of the band gaps can shift due to

deformations of the crystal structure. The structure of the photonic crystals can be deformed by the effects of strain, thermal expansion, and other effects. These shifts are to be calibrated to be used as a monitoring system. This monitoring system will be utilized in real time to assess stress and strain in a nuclear reactor on the various reactor components.

Photonic Crystal Fabrication

Photonic crystals are engineered structures of periodic material that can be written on many different types structures of interest. The photonic crystal used for this project is a square lattice of steel pillars surrounded by air that were fabricated using a focused ion beam or FIB. The FIB used to produce the photonic crystals for this project, as shown in figure 2, works by shooting gallium ions at the surface of the sample and sputtering away material [4]. This sputtering away of the material allows for the creation of new structures of periodic material, which, in this case, are pillars of steel surrounded by air.

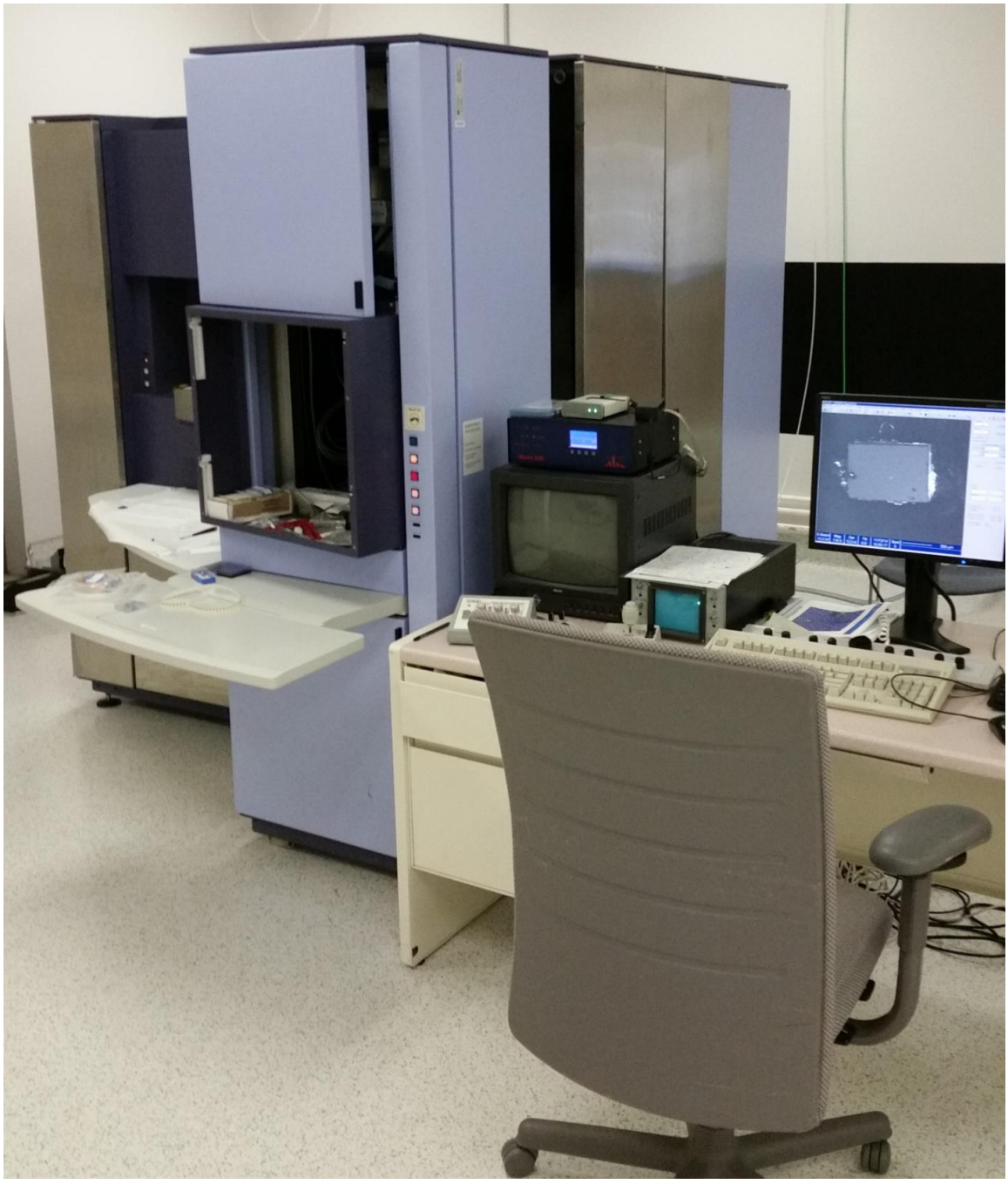

Figure 2: Dual beam FIB which was used to produce the photonic crystal used in project [5]

The advantage of using the FIB was that photonic crystals could be prototyped easily on different materials and also made very small. The processes for engineering structures in Silicon are well understood, but not as much as other material of interest. The ability to create small crystals allows for location specific applications such as placement on grain boundaries. Figures 3 shows the images of the crystal produced by the FIB and used for interrogation in this paper. A honeycomb lattice is the optimal lattice structure, but a square lattice of pillars was used due to the ease of fabrication.

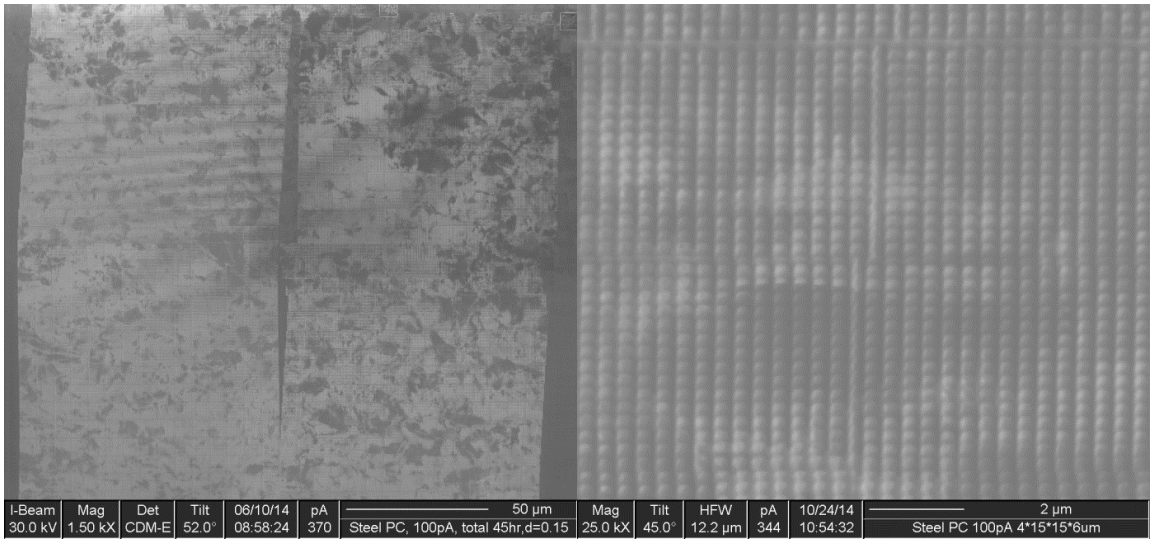

Figure 3: Images of the photonic crystal used for this project [1]

Interrogating Crystal Off Axis

The photonic crystals used for this project are two-dimensional, meaning they are periodic on two axes. While two-dimensional crystals are theoretically infinite on the third axis, crystals in real life cannot be infinite and are built large enough the finite height can be neglected [3]. Previous simulations and experimentation for two-dimensional crystals have been completed mainly within the plane that the crystal is

periodic. For the light gauge application, this periodic plane is not accessible to the light source and detector. Some testing has been completed off axis on a two-dimensional crystal [6]. However, it is unclear how the crystal behaves in a steel substrate. A custom test stand was designed and built to interrogate the crystal response out-of-plane.

Theory

Photonic Crystal Basics

Photonic crystals are periodic structures of dielectric material. When the dielectric properties of the materials contrast enough, band gaps will form. Typically the greater the dielectric contrast of the materials, the larger the band gaps are. Band gaps can form in either transverse-magnetic (TM) or transverse-electric (TE) polarizations of light. Complete band gaps form when TM and TE band gaps overlap. Photonic crystals can be periodic in one, two or three axes, depending on their structure and are correspondingly referred to as one, two or three-dimensional crystals. Figure 4 illustrates the three different types of crystals. [3]

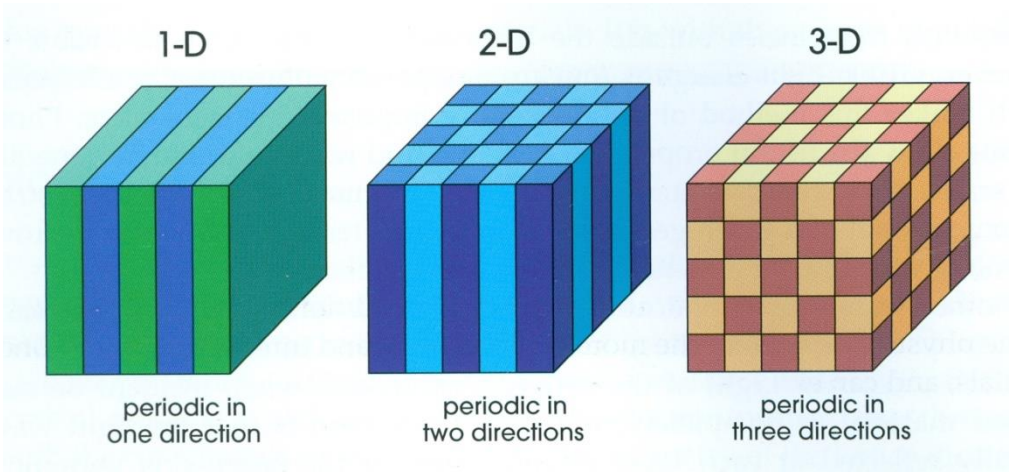

Figure 4: 1D, 2D and 3D photonic crystals [3]

The simplest form of a photonic crystal is a 1D crystal, which alternates layers of contrasting dielectric material on a single axis, also called a multilayer film. A diagram of a 1D multilayer film is shown in figure 5. A Bragg mirror is one example of such a structure and acts as a mirror for specific frequencies of light. [3]

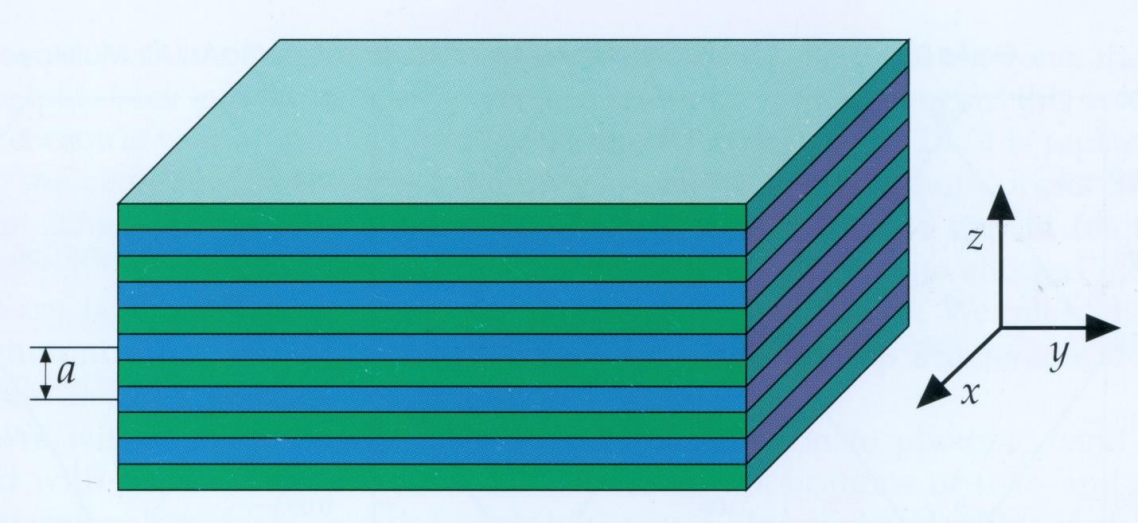

Figure 5: 1D Photonic crystal also known as multilayer film [3]

2D Crystals

The dielectric materials of 2D crystals are periodic on two axes and homogenous in the third. No band gaps are experienced on the third axes. There are many different types of structure possibilities for 2D crystals, each with different behaviors. The rule of thumb, as set out by Joannopoulos, is that "TM band gaps are favored in a lattice of isolated high dielectric regions, and TE band gaps are favored in a connected lattice" [3] [7]. Figure 6 shows three different photonic crystal structures that demonstrate how this principle is applied. The first lattice on the left in figure 6 is a square lattice of columns made from dielectric material surrounded by air. The square lattice favors TM

band gaps because the columns consist of isolated regions of high dielectric material. [3] [7]

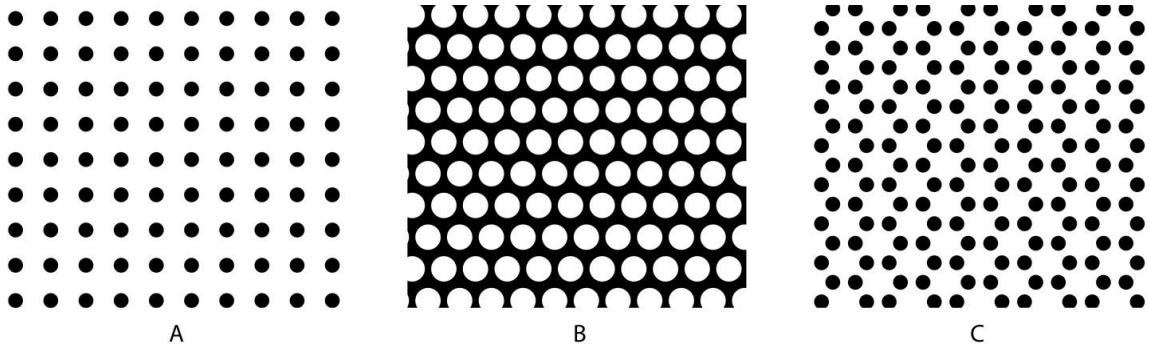

Figure 6: 2D crystal lattices: square, triangular and honeycomb lattices

The center lattice in figure 6 is a triangular lattice of air columns in a dielectric substrate. This triangular lattice structure is a compromise between a lattice of isolated regions of high dielectric material and regions of connecting lattice. The spots between the air columns resemble regions of isolated high dielectric material and at the same time are connected together by veins of dielectric material at the narrow sections between air columns. Figure 7 illustrates where these spots and veins of high dielectric material are located in the lattice structure. This structure is capable of producing a complete band gap as a result of the compromise. [3] [7]

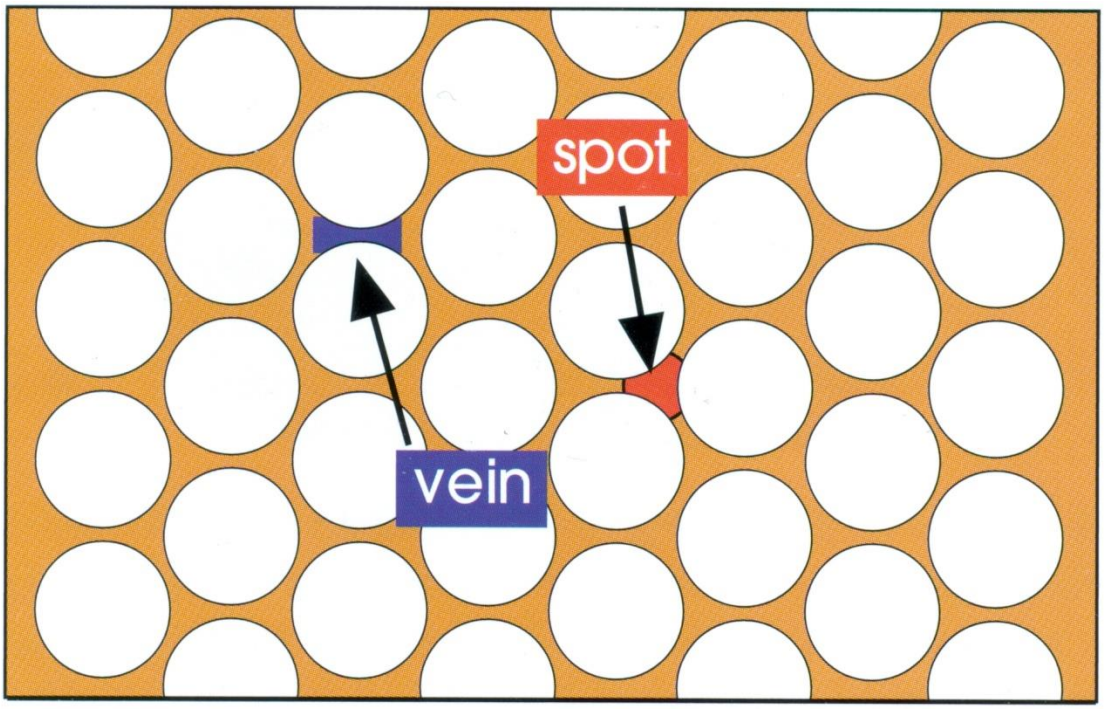

Figure 7: Triangular lattice of a 2D photonic crystal [3]

The final lattice on the right in figure 6 is a honeycomb lattice of columns made from dielectric material surround by air. The honeycomb lattice is like the triangular lattice in that it can produce a complete band gap, but the band gaps are larger and at higher modes [8]. The advantage of this lattice structure is that it is easier to manufacture than the triangular lattice [3]. This is because the feature size of the veins in the triangular lattice to produce a complete band gap would be small enough to create difficulty. [3]

3D Crystals

The dielectric materials of 3D crystals are periodic on all three axes as shown in figure 4. This periodicity enables a complete band gap to form on all three axes [3]. While the 3D crystal exhibits the ideal properties for a photonic crystal sensor, they are also currently too difficult to manufacture for the LightGauge application. Since 3D crystals are unable

to be used, two dimension crystals must be used and their response between axes understood.

Methodology

Hypothetical World

Ideal Setup

The first step to understanding how to design a new instrument that will interrogate the emission response of a 2D photonic crystal was to describe the desired experiment in an ideal world. In this ideal world, the new instrument should be able to measure the crystal response at any angle relative to the incoming beam from the light source. The point of collection of the crystal response and the point of origin of the light source will move around the crystal as if on the surface of a sphere. The radius of this sphere should be held constant as the instrument is moved about the crystal so that data collection is not affected by a change in intensity of the light source as a result of a non-constant distance from the crystal. The collection point should also be infinitesimally small with infinite precision so as to give the greatest granularity. [9]

Assumptions for Real World Application

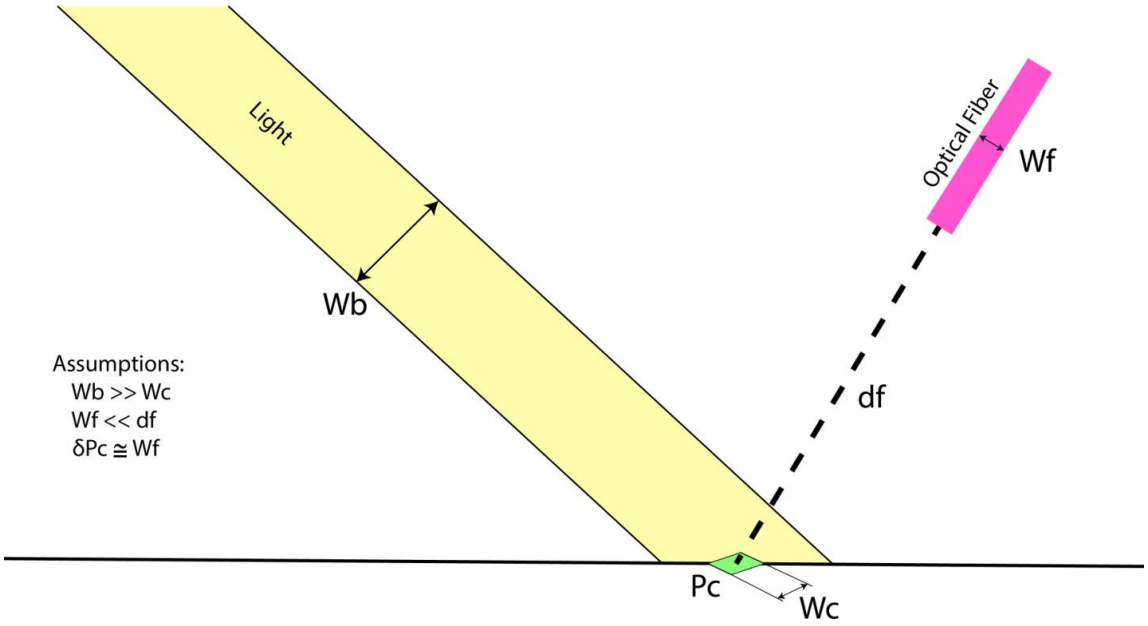

Figure 8: Diagram of assumptions

The real world of a crystal measurement is not ideal, so a number of assumptions were made to compensate. The first assumption was that the width of the beam from the light source shining on the crystal is much greater than the width of the crystal. This allows the crystal to move in the plane and not be affected by the size of the beam. If the source beam were too small, imperfections in the crystal structure could cause the emission response of the crystal to vary as the beam shines on these imperfections. The second assumption was that the width of the collection fiber should be much less than the distance of the fiber to the crystal. This is primarily for angular resolution but also so that all incoming rays of light can be assumed to have the same acceptance angle into the collection fiber. The third assumption was that the change in the crystal position during the measurement needs to be about the same as the width of the fiber. This assumption minimizes changes in crystal response that would result from changes in the

crystal position instead of the fiber position. The last assumption was that the crystal response in the surrounding space is symmetrical. The crystal response would not be required to be measured at every possible location but can be limited to one-half of a particular symmetry. The first three assumptions are depicted graphically in figure 8. [9]

Design Considerations

Collection Point of the Emission Response from the Crystal

The crystal's emission response cannot be collected at a single point in space, but it can be collected over an area. An optical fiber was used to collect the crystal response over an area represented by the cross-sectional area at the end of the fiber. The spectrum of the crystal response then travels through the fiber to a spectrometer to be measured. There are some tradeoffs entailed in the selection and use of an optical fiber. When comparing optical fibers of varying widths, a fiber with a larger diameter will have a larger area and collect a higher intensity of the crystal response. This comes at the expense of the resolution of the spectrum because the spectrum is collected at a larger solid angle. The distance between the crystal and the fiber can be increased to offset the increase of a larger solid angle because light obey the inverse square law [10]. Doing so, however, results in another tradeoff. The intensity of the measured crystal response will lose the gained intensity from increasing the width of the optical fiber. The distance between the crystal and the fiber can also be increased by increasing the integration time of the spectrometer, but more noise enters the system as the integration time is increased.

Experiment Coordinate System Definition

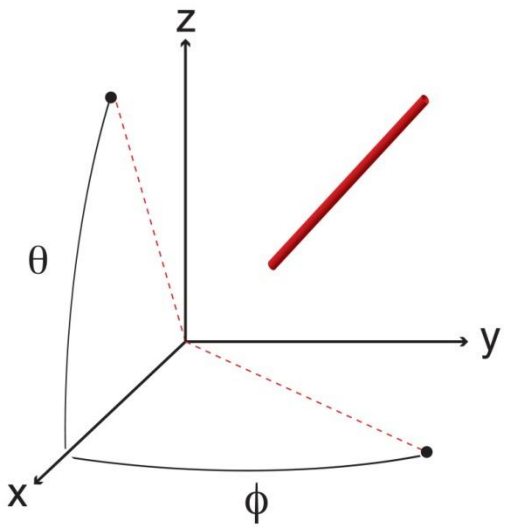

Figure 9: Coordinate system definition

Figure 9 shows the coordinate definition system that was used throughout the experiment. The crystal location remaining fixed in space is desirable as the point from which the spectrum of the crystal response is collected and moved around the crystal. The crystal response was collected by a fiber that is represented by the pink tube which was kept at a constant distance from the crystal as its location is varied. Theta and Phi represent the way in which the collection fiber or crystal may be rotated to measure the crystal response at different locations. Understanding several concepts is essential to the application of this coordinate system. These concepts are eucentric height, the order of stages and the modified XRD stand design that was used in the design.

Eucentric Design

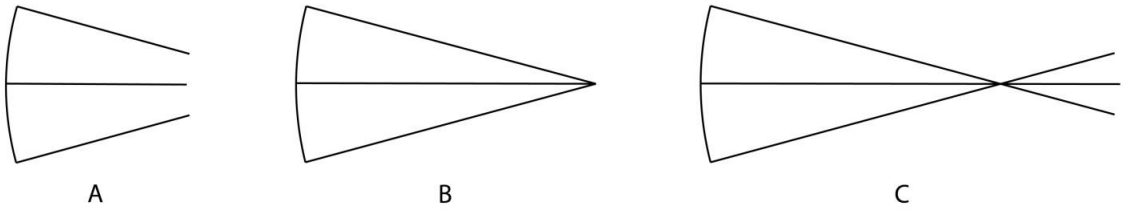

Figure 10: Eucentric height

The rotation of the fiber or light source can be simulated by simply rotating the crystal instead. The key to this simulation is that the location of the crystal must remain fixed in space as it is rotated. Using a eucentric cradle is one method of rotating the crystal while keeping its location fixed in space. The cradle functions by placing the surface of the sample at the eucentric height. Eucentric height means that the specimen height is adjusted to be on the tilt axis of the cradle stage [11].

Figure 10 shows three arcs, each representing a cradle with a stem that is rotated to three positions. The height of each stem for each arch remains constant as it is rotated. Example A of figure 10 shows that when the stem height is shorter than the tilt axis, the tip of the stem changes position as it is rotated. The tip of the stem also changes position when the stem is longer than the tilt axis, as shown in example C. Only when the stem height matches the tilt axis height will the position of stem tip remain constant, as shown in example B.

The knowledge that the tip of the stem moves when the stem height does not match the eucentric height can be used to determine the eucentric height. This is

accomplished by incrementally adjusting the height of the stem of a cradle and then rotating it until the tip the stem no longer moves [11]. In practice, when the eucentric height is found for a eucentric cradle, the crystal also has to be translated on the XY plane of the sample it is located on so that it is located on the tilt axis in addition to the surface of the sample.

Order of Stages

The order of the stages is important when the crystal's position needs to be maintained during its rotation. Multiple cradles stacked on top of each other are required to rotate the crystal about multiple axes. These cradles also have to be aligned correctly otherwise additional positioning stages will be required for each rotation stage. Two examples are given which illustrate these conditions.

The first example, as shown in figure 11, has a cradle stacked on top of the stem of another cradle. The heights of both cradles are adjustable and are identified by Z_1 and Z_2. The bottom cradle, to the left in the figure, has a larger arc than the inside cradle.

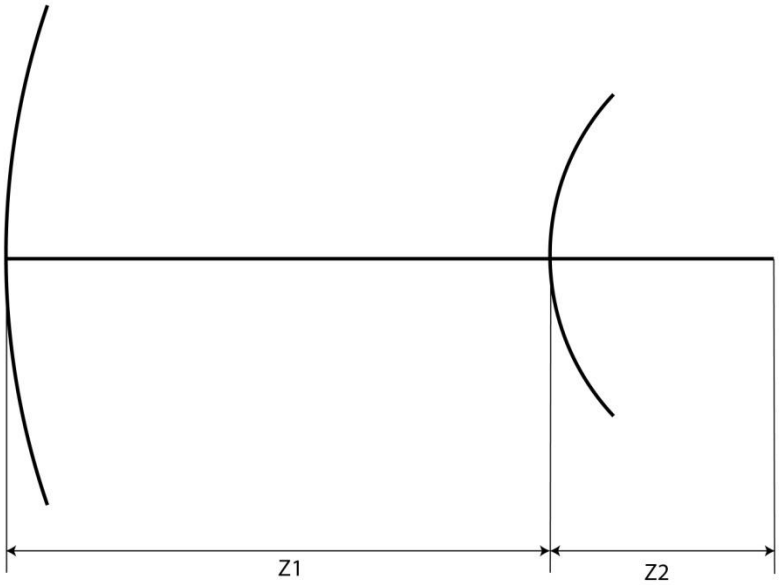

Figure 11: Multiple stages

The adjustment of the stem height Z_1 will allow the tip of the stem of Z_2 to be eucentric for the first cradle but not necessarily for the second cradle. Only by adjusting both stem heights can the eucentric height for both cradles be found. If Z_2 is not adjustable and fixed to the correct length, only Z_1 is required to be adjusted.

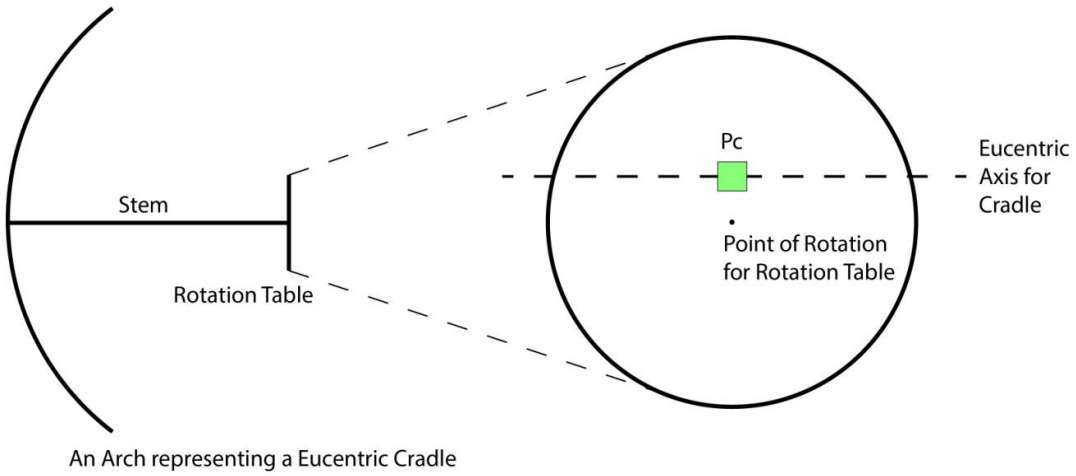

Figure 12: Example 2 of why stage ordering matters

The second example is of a rotation table attached to the stem of a eucentric cradle. The rotation table rotates about an axis within the plane of the surface of the rotation table, as shown in figure 12. Although not shown in the figure, there is placed on top of the rotation table an XY translation stage and then a sample that has a photonic crystal written on its surface. The XY stage allows the translation of the crystal to be positioned on the tilt axis. The figure reveals the condition when the center of the rotation table is not aligned with the rotation axis of the cradle. The crystal can be positioned using the XY stage on the tilt axis of the cradle or the center of the rotation table but not both locations at the same time. If the photonic crystal is positioned on the axis of the cradle instead of the center of the rotation table, the photonic crystal position will move every time the rotation table moves and vice versa. Having an XY stage on both the stem of the cradle and on top of the rotation table will allow for rotation of the cradle and rotation table without changing the crystal's position when the axis of the rotation stage is not aligned with the tilt axis of the cradle.

Stand Design

Modification of an XRD stand

The new instrument design modified an old XRD stand for the purpose of the experiment. The unmodified XRD stand allowed for rotation of a sample around multiple axes and a viewing optic for centering the crystal at the center of the system. A rotation arm was added for rotating the collection fiber of the crystal's emission response. The new custom test stand incorporates two experimental setups.

Bottom Rotation Table

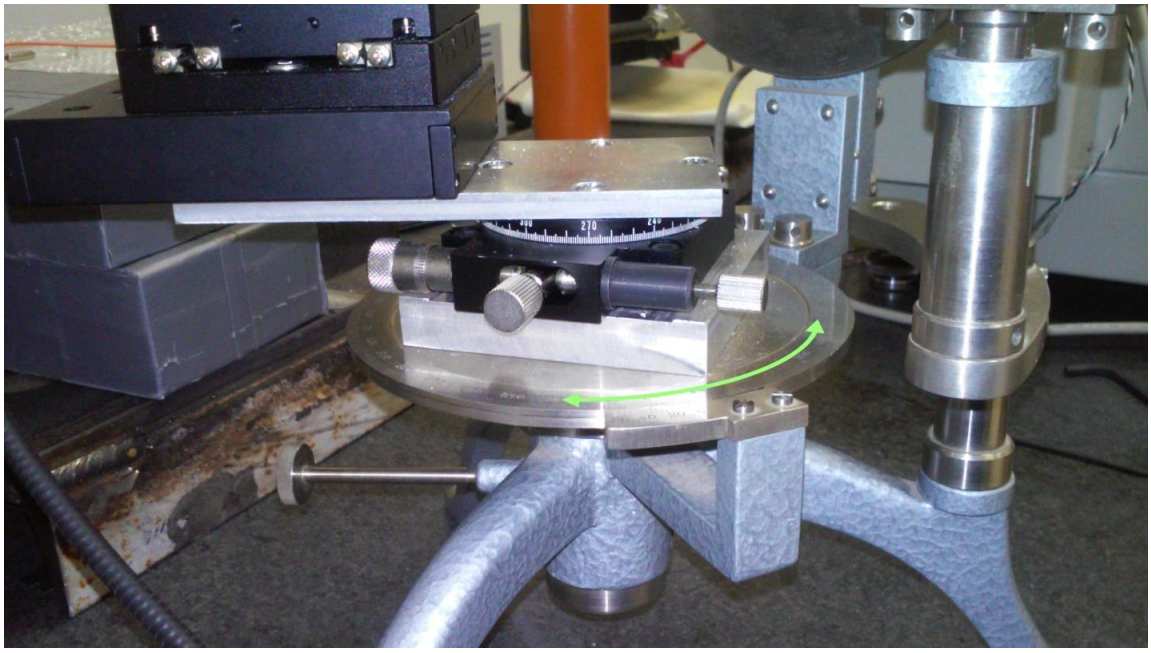

Figure 13: Bottom rotation table

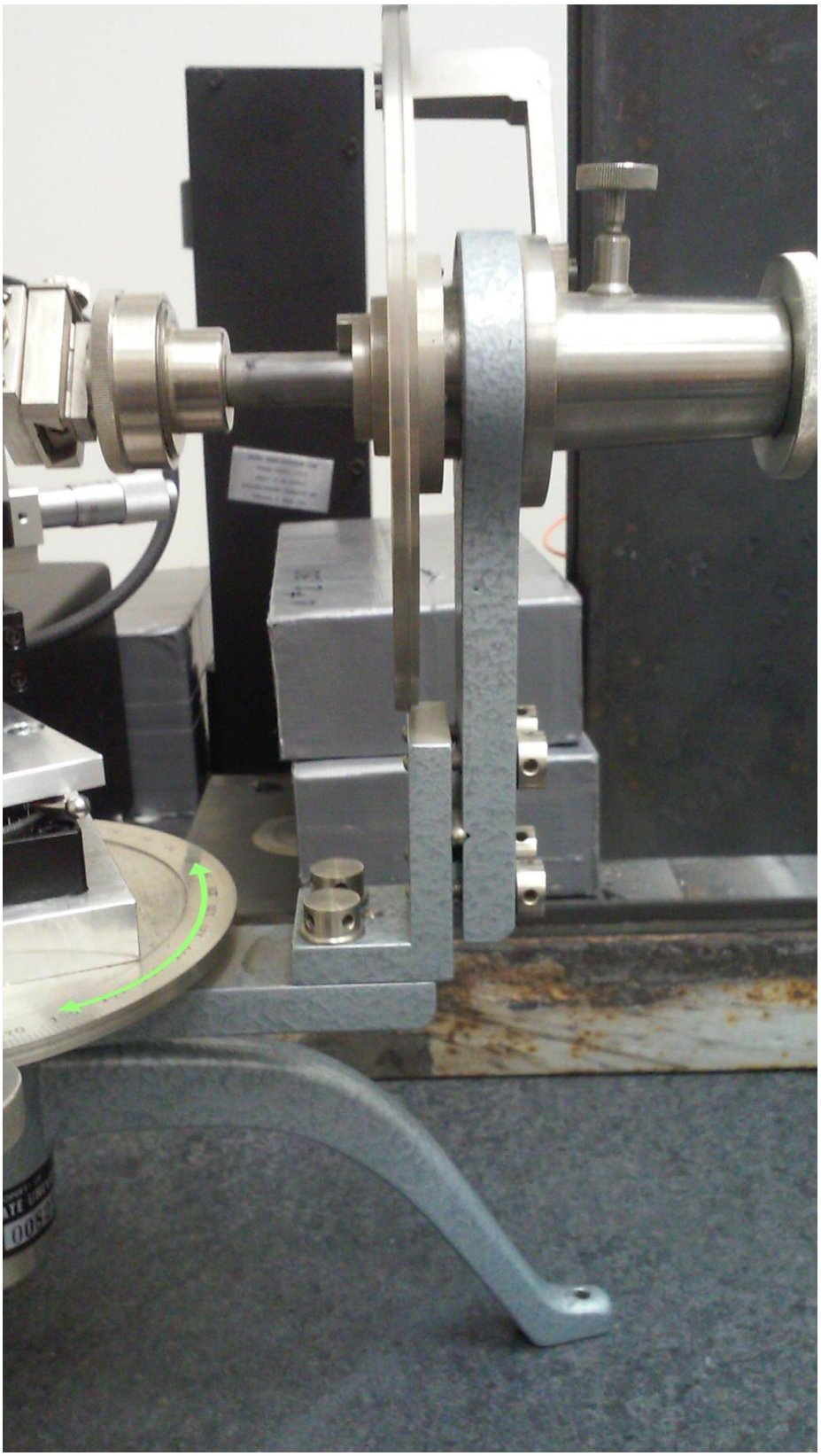

Figure 14: Arm extended from bottom rotation table

At the bottom of the XRD stand is a rotation table that allows for rotation about an axis in a plane. An arm is then attached to the edge of the rotation table that shoots up vertically and then points back toward to the axis of rotation. This arm can be seen in figure 14. A series of stages are attached to this arm that allows for additional rotation and positioning of the sample with the photonic crystal. The bottom of the arm allows for adjustment of the direction of the first stage attached to the arm. This allows the stage to be aligned so that it points to the tilt axis of the bottom rotation table.

Sample Arm

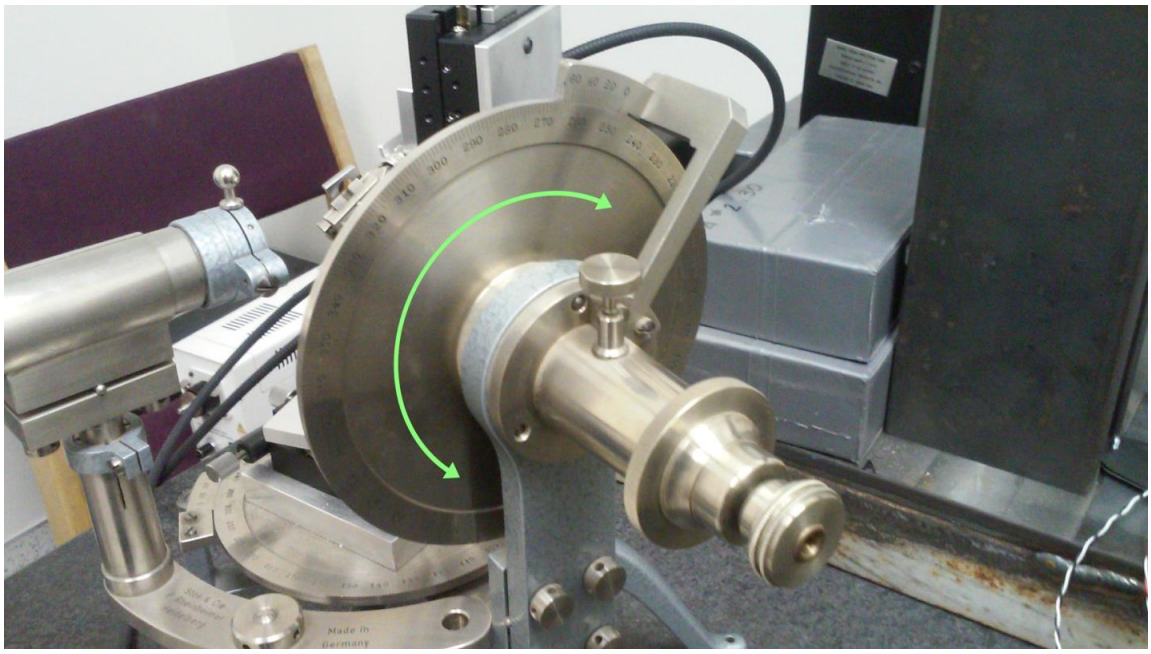

Figure 15: Sample rotation table

The arm with a series of stages that are attached to bottom rotation table that allows for rotation and positioning the sample is called the sample arm. The first stage attached to the sample arm is a rotation table that allows for rotation within a plane of the sample about an axis. This rotation table is called the sample rotation table. The

rotation table has a micrometer attached to it that allows for the angle of rotation to be measured with 1 degree resolution plus or minus a quarter of a degree.

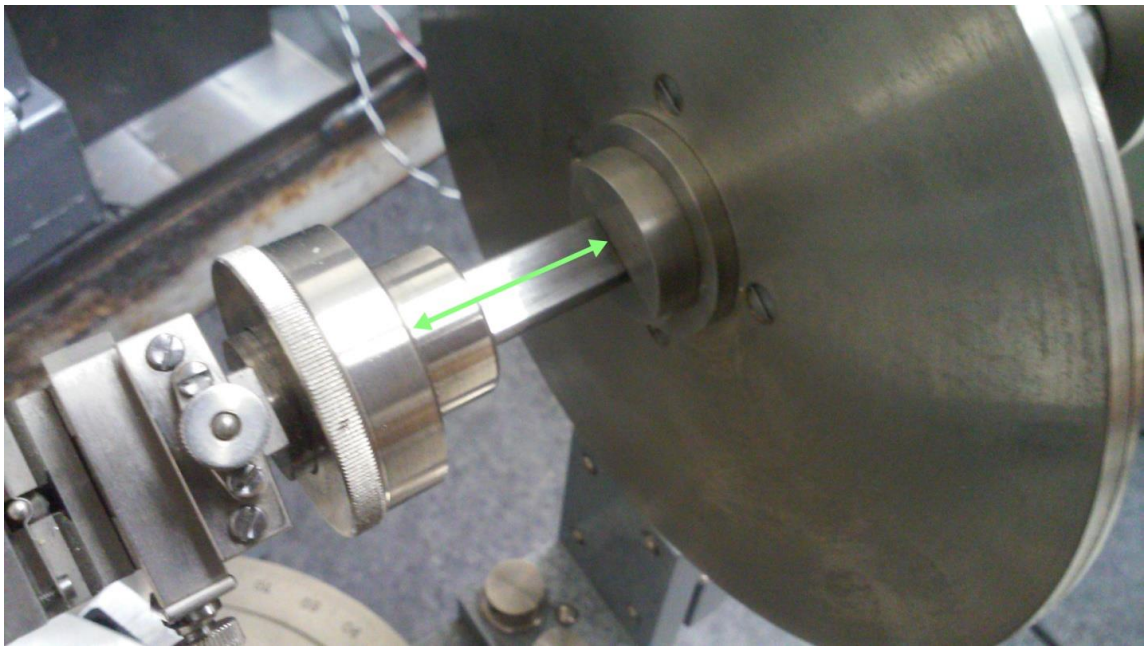

Figure 16: Z movement

After the sample rotation table is an arm that drives the movement of the sample depth as shown in figure 16. This is called the Z drive and allows the sample to be positioned at the eucentric height of the bottom rotation table. The depth adjustment is made using a knob behind the sample rotation table.

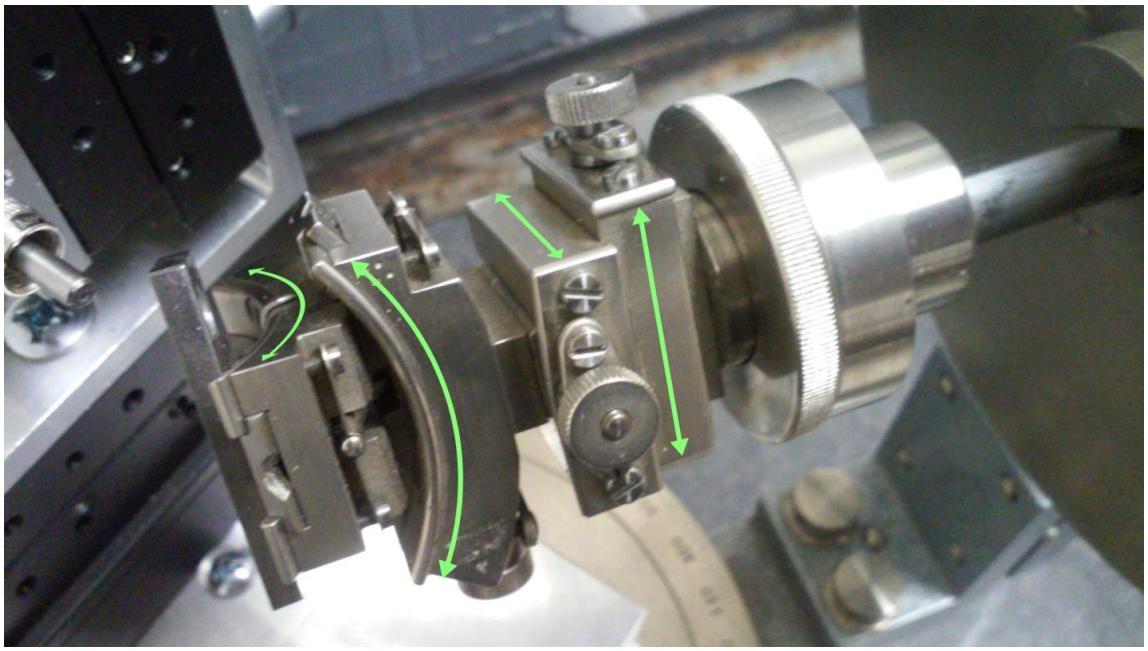

Figure 17: Sample arm with the rotation and position stages for the sample

The next stages on the sample arm are two XY translation stages followed by two cradles which rotate about the X and Y axes. These stages on the sample arm are shown in figure 17. The two cradles support a total of 20 degrees of rotation at 1 degree resolution and ½ degree accuracy. The XY stages do not have a micrometer reading on it.

There are no adjustments for the height of the sample from inside the cradle. The last cradle does have a hole where a stem can be inserted to achieve the eucentric height of the two cradles. If no stem is used, the Z drive can be used to obtain the eucentric height of the bottom rotation table, but the eucentric rotation of the two cradles on the sample arm will be lost.

There are also no XY translation stages inside of the cradles. These stages are required to position the photonic crystal on the eucentric axis of the cradles once the eucentric height has been obtained. However, carefully attaching the sample to the stem can simulate another XY translation stage to position the crystal relative to the two cradles. Although the XY translation stages do not position the crystal relative to the two cradles, it can be used to position the crystal relative to the eucentric axis of the bottom rotation table (once the eucentric height has be obtained) and the rotation axis of the sample rotation table.

Rotation Arm for Collection Fiber

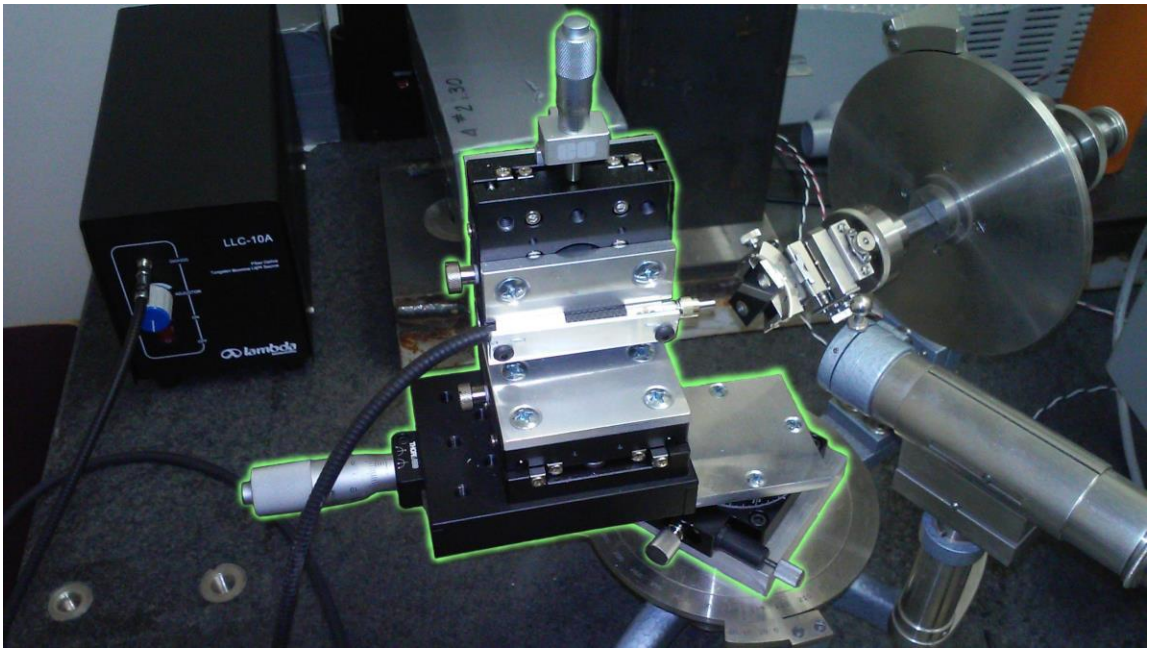

Figure 18: Fiber rotation arm which rotates the collection fiber around the crystal at a fixed distance from the crystal.

A fiber rotation arm was designed and added to the XRD stand so that the collection fiber is able to rotate around the crystal at a fixed distance away from the crystal. The arm uses a series of translation and rotation table stages mounted on custom designed

parts to rotate the fiber. The center of rotation of the arm was aligned to match that of the bottom rotation table. This enables the crystal to remain eucentric to both the sample arm and fiber rotation arm without changing the crystal's position in space. The rotation arm can move 360 degrees of rotation but is limited in its motion because the sample arm and optical viewing piece are in its path of motion. The rotation of the fiber is also confined to within a plane, and all rotation outside of this plane is simulated by rotation of the photonic crystal.

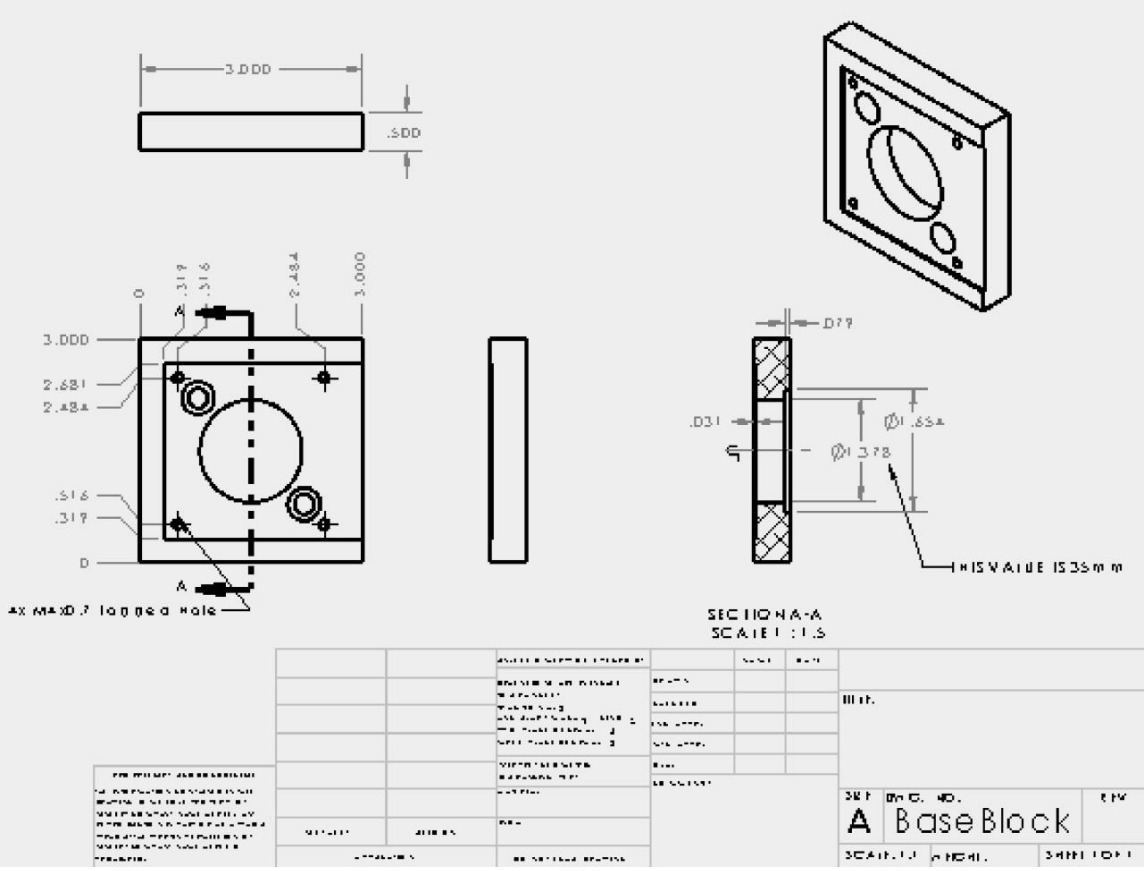

Figure 19: Base plate drawing. The base plate provides an elevated surface for the fiber rotation table to attach to and aligns the axes of the fiber rotation table and the bottom rotation table to be collinear

The first stage of the fiber rotation arm is a rotation table that attaches to the bottom rotation table of the XRD stand with a custom adapter. This rotation table is referred to as the fiber rotation table and is able to rotate 360 degrees. An adapter is required because part of the surface of the bottom rotation table protrudes upward in the shape of a cylinder creating difficulty in attaching the fiber rotation table. The adapter is referred to as the base plate and provides an elevated surface above the cylinder for the fiber rotation table attaches to.

The base plate also aligns the two rotation axis of the two tables together to be collinear. This is accomplished by designing a hole into the base plate to fit around the cylinder. This center of the hole then becomes a reference point for the center of the bottom rotation table because the center of the cylinder is also the center of the bottom rotation table. A recess at the top of the base plate then positions the fiber rotation table to be centered on the hole in the base plate thereby centering the fiber rotation table on the cylinder of the bottom rotation table. The design of the base plate is shown in figure 19.

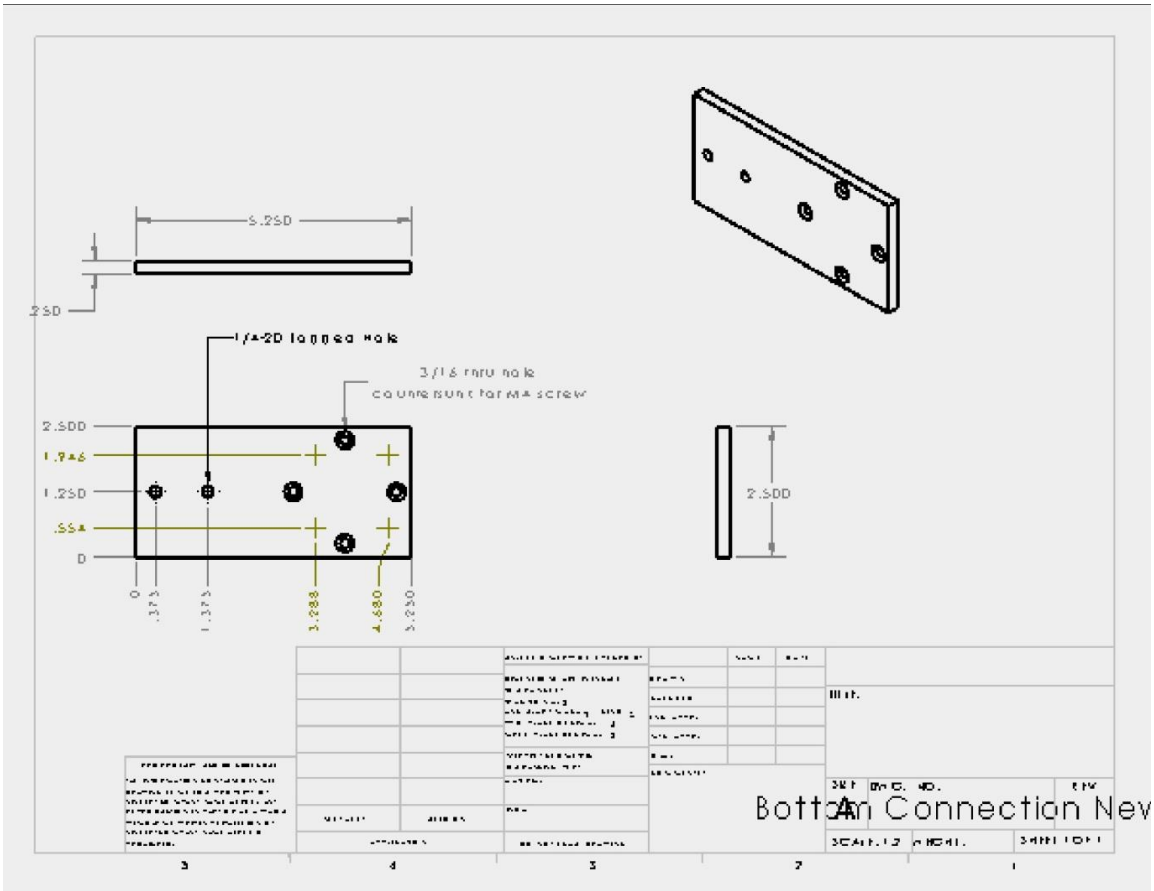

Figure 20: Drawing of bottom connection arm that attaches to the fiber rotation table. The arm allows the fiber to rotate about the axis of rotation of the fiber rotation table from a distance

An aluminum plate is attached to the rotation table that forms an arm which allows the fiber to rotate about the axis of rotation of the fiber rotation table from a distance. This arm is referred to as the rotation arm plate and is shown in figure 20. Three translation stages are attached to the top of the rotation arm plate that gives the sample travel on three separate axes that are normal to each other. This allows the fiber position relative to the rotation arm plate to be adjusted.

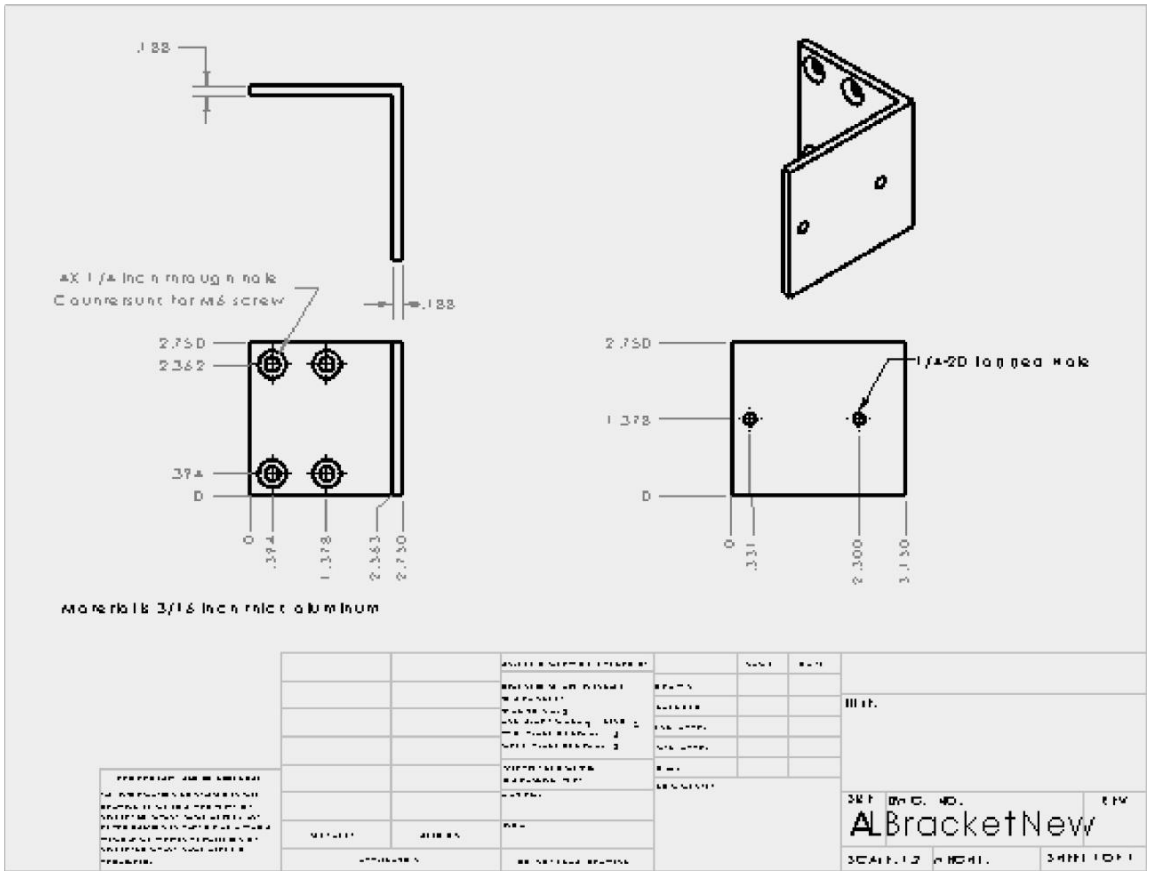

Figure 21: Drawing of bracket used to attach the two translation stages on the X and Y axes

The first translation stage attached to the top of the rotation arm plate is called the Z stage. The direction of travel of the Z stage is collinear to the rotation arm plate thus pointing it toward the center of rotation of the fiber rotation arm. The next translation stage is attached to the top of the Z-stage parallel to it and is called the X stage. The direction of its travel is perpendicular to that of the Z stage. The last translation stage is called the Y stage is positioned on the third axis perpendicular to both the Z and X stages. In order to attach the Y stage perpendicular to the other stages, a bracket was designed that attaches to the top of the X stage and provides a place for the Y stage to attach to.

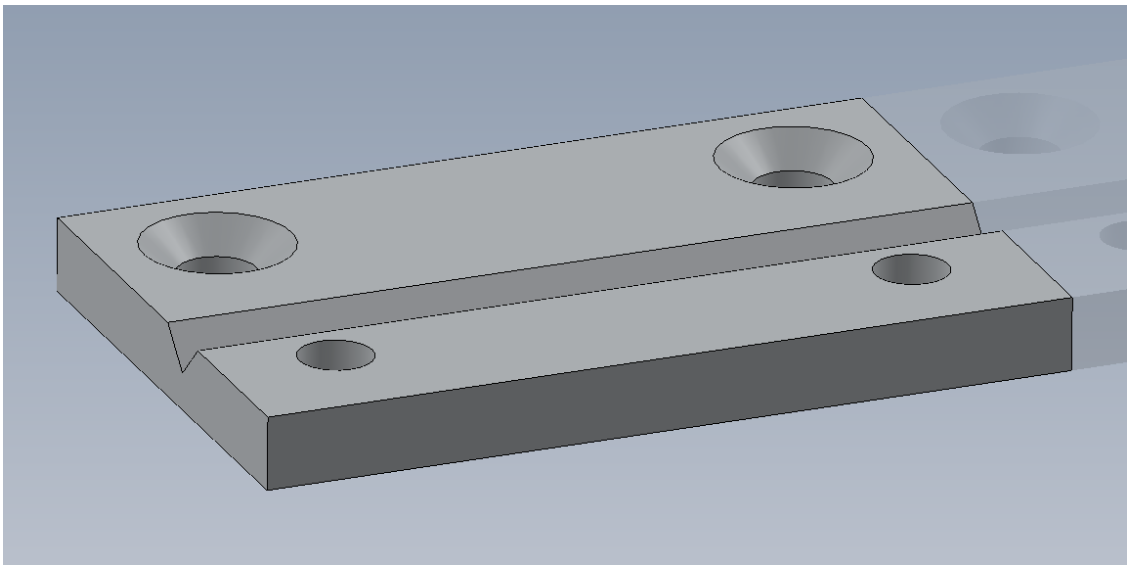

Figure 22: Fiber connector plate used to hold the fiber in place

Lastly, an adapter plate is attached to the Y stage to hold the fiber in place. The adapter plate uses a V-groove that positions the fiber in the correct position. The fiber is held in the V-groove using another plate which tightens down on the fiber.

Optical Viewing Piece

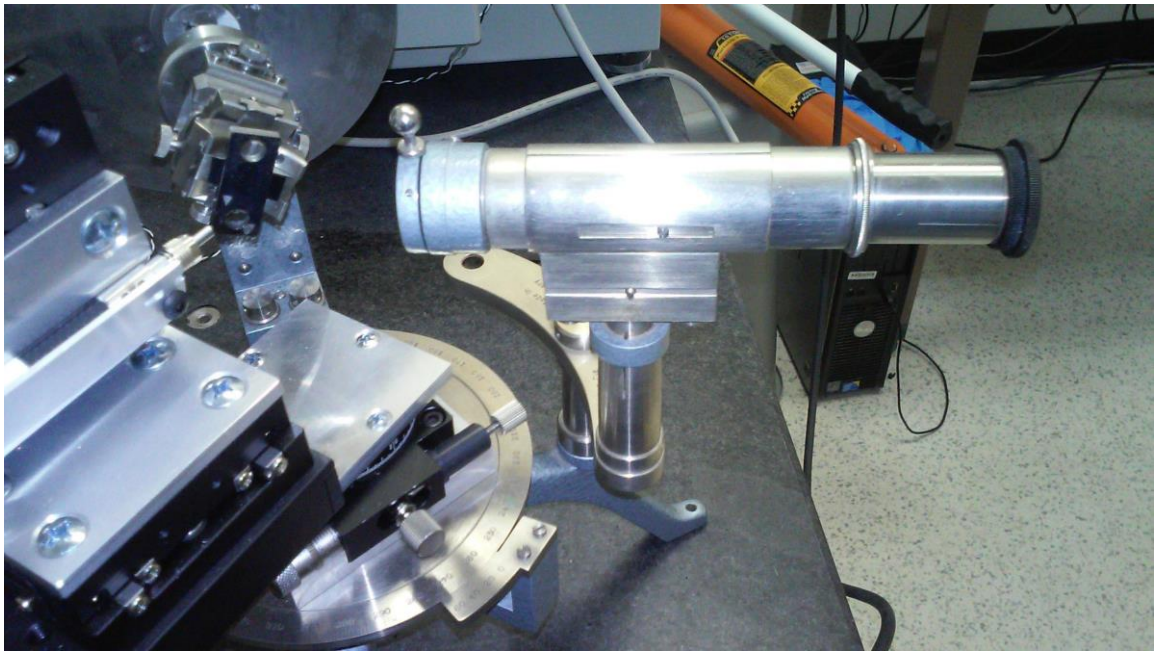

Figure 23: Viewing optic of the XRD stand

Part of the XRD stand is a viewing optical piece that points to the center of the system. This optical viewing piece is used for positioning the crystal in the center of the system. The idea is to rotate one part of the system at a time and see if the crystal has moved. If the crystal has moved, adjustments to one or more of the stages on the stand are made until the crystal no longer moves. Because the optical piece points to the center of the system, it can also be used as a light source by shining light through the optical piece.

Original Setup

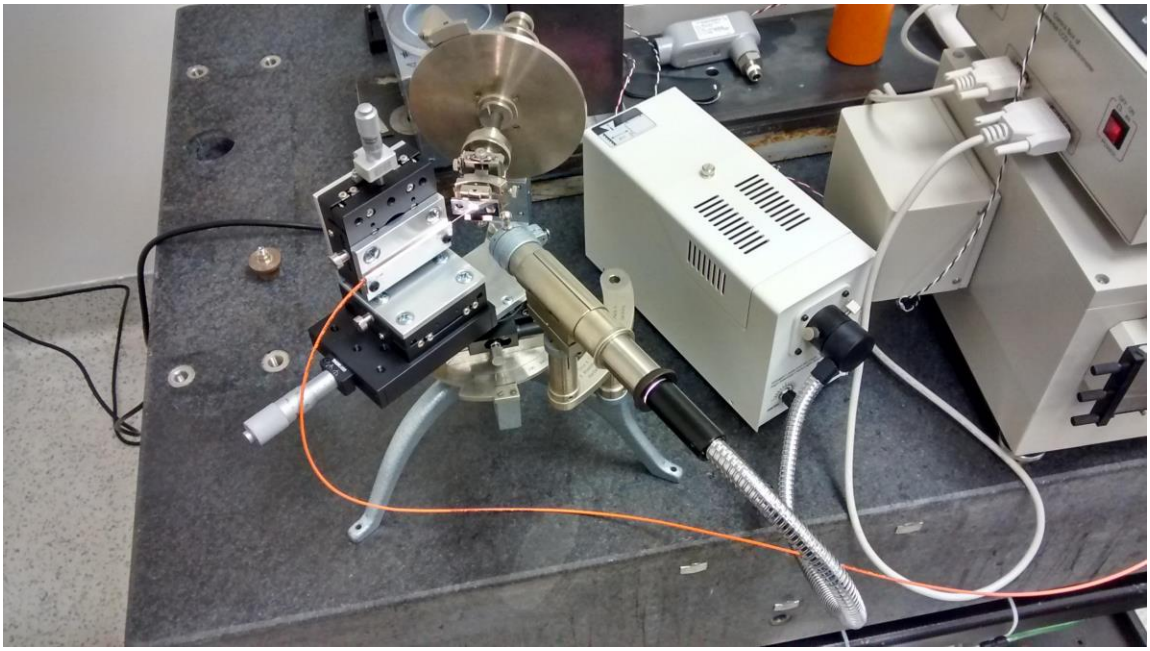

Figure 24: Original experimental setup using a fiber optic cannula as the collection fiber and the light source sent through the viewing optical piece of the stand

The stand can support two experimental setups. The first setup uses a fiber optic cannula attached to an optical fiber for the collection fiber. Light from a halogen bulb is sent through the optical viewing piece for a light source. Although the optical viewing piece is at a fixed location, its movement is simulated with crystal rotation. The light source and fiber are always in the same plane. This setup was used for most of the early tests including most of the spectrometer calibration.

Final Setup

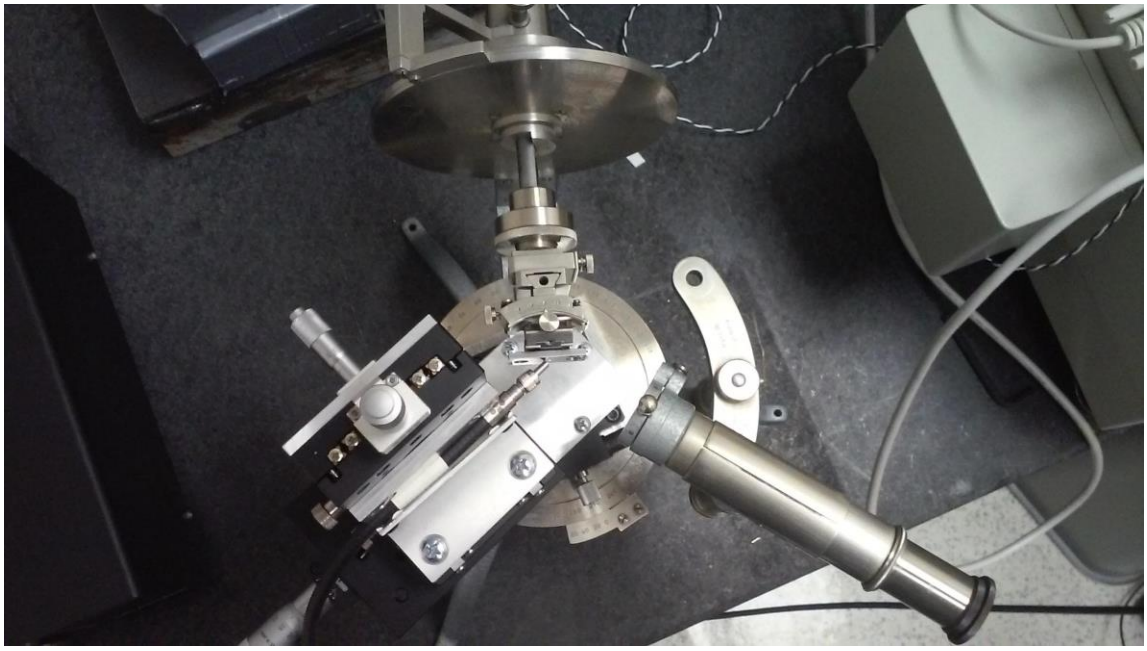

Figure 25: Final experimental setup using a reflection probe for a collinear light source and collection fiber

The final setup uses a collinear light source and collection fiber. This is done by using a reflection probe that contains multiple fibers bound together. The center fiber is used as the collection fiber of the emission response from the crystal and is sent to the spectrometer. The surrounding six fibers provide light from a tungsten bromine light source. Using the reflection probe not only simplified the experiment but potentially provides more useful information. This is because positioning two fibers instead only one around a crystal in a real world application is potentially more difficult. The final setup does not require the use of the last two cradles on the end of the sample arm. All rotation of the crystal was accomplished using the sample rotation table and the bottom rotation table.

Calibration of Spectrometer

Background and Source Measurements

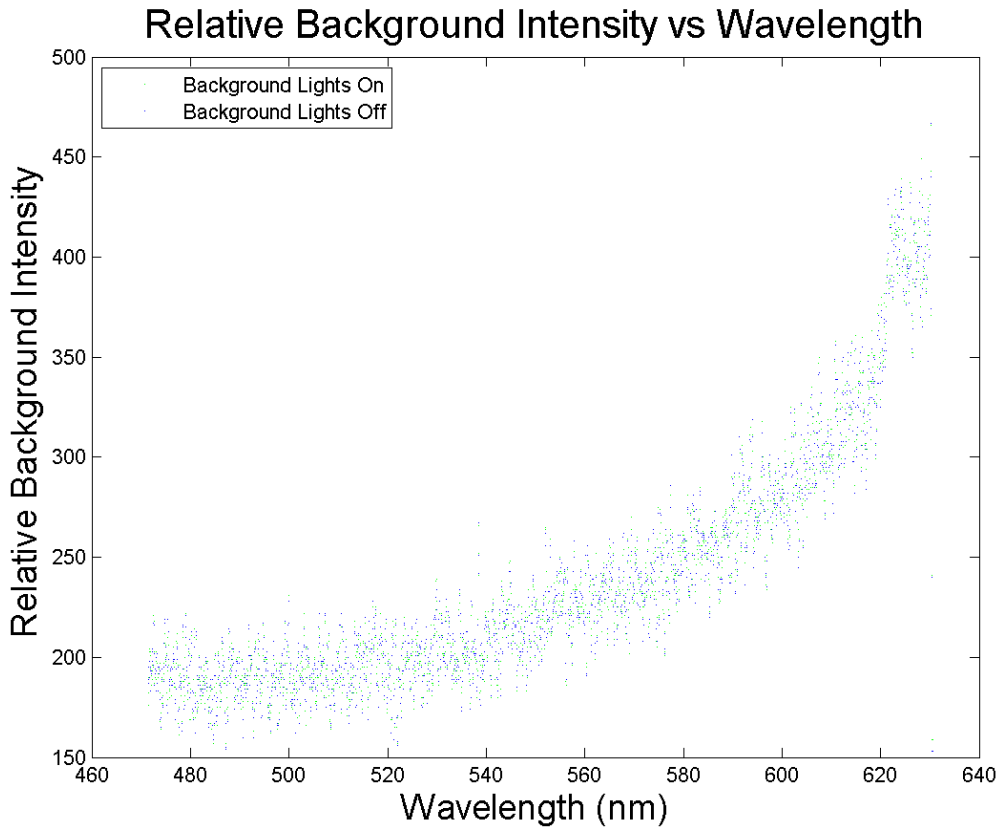

Figure 26: Effect of room lights on and off

The effect of the room light on any given measurement using a spectrometer was investigated by taking the measurement of a spectrum entering the fiber with the room lights on and off. The results are shown in figure 26 and show that the room light does not have an appreciable effect on a spectrometer measurement. It also shows that there is a structure in the spectrometer reading not created by the spectrum it is measuring. This structure will need to be subtracted out from each reading.

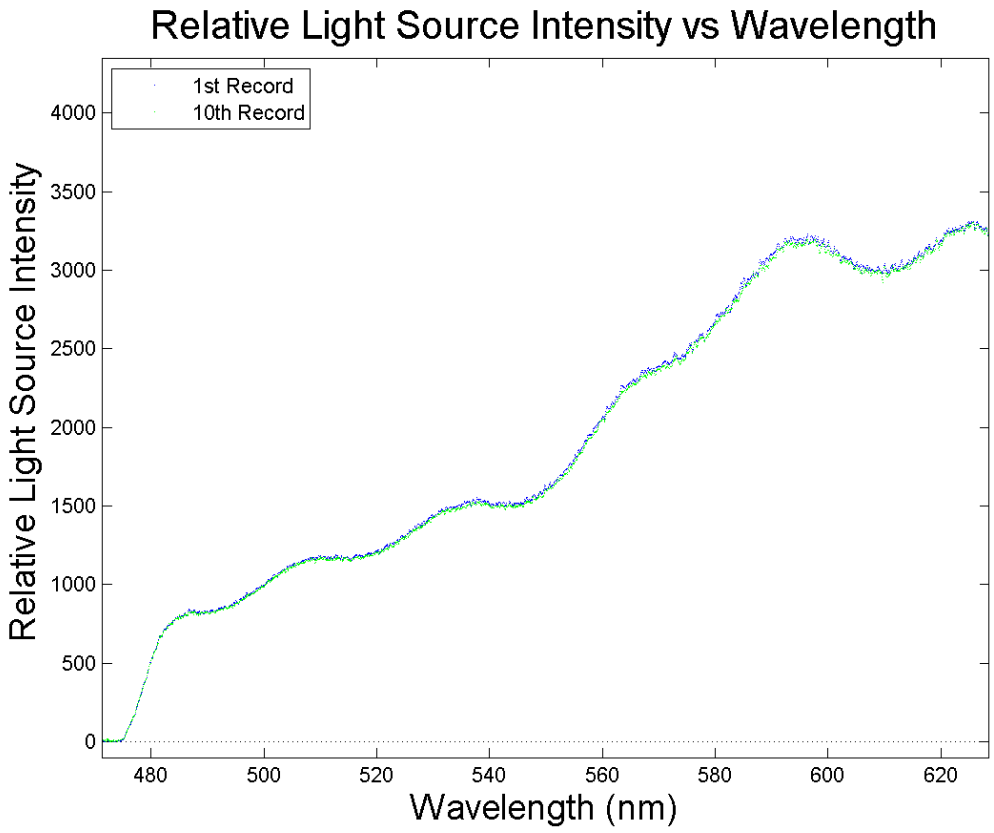

Figure 27: The first and tenth measurement of a light source

The repeatability of a spectrometer measurement of a light source without any setting changes to the light source or the spectrometer was investigated. The first and tenth measurement of the light source spectrum is shown in figure 27. It was found that there were no appreciable differences.

Fiber Alignment Tool for Spectrometer

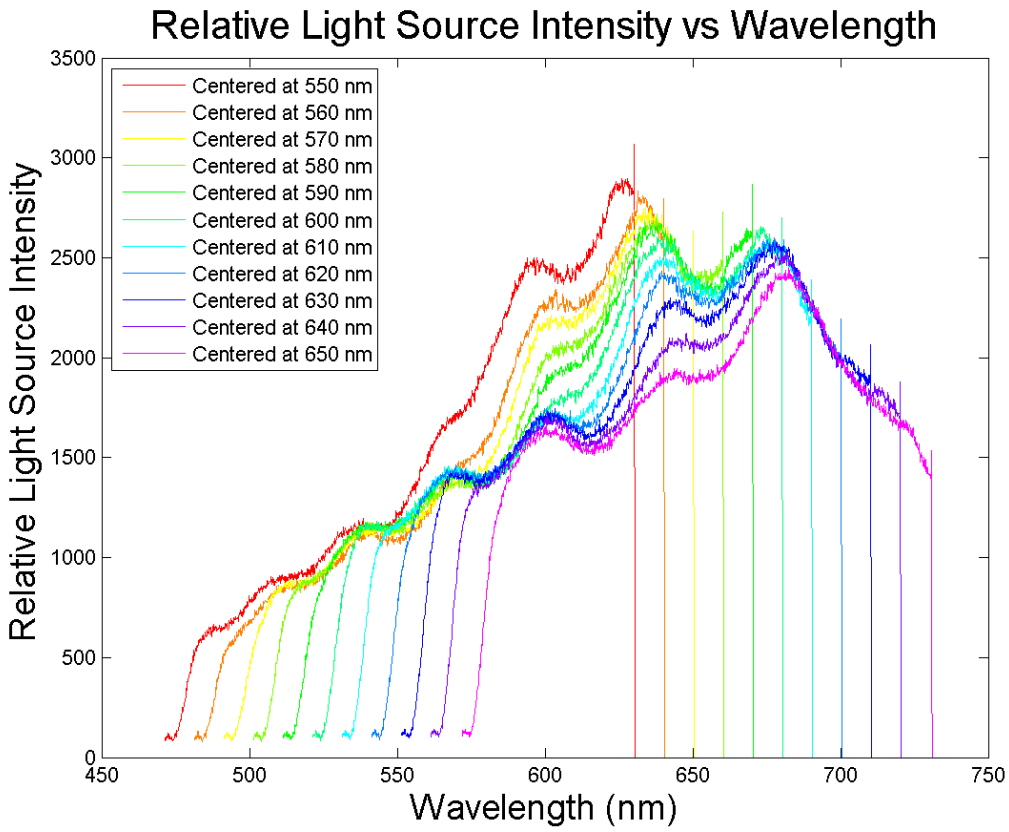

Figure 28: Light source spectrum measured as the spectrometer window is moved

It was desired to understand how changing where the spectrometer window of measurement is centered affects the measurement of a spectrum. This was done by measuring the light source reflected off of steel while changing the window's center wavelength by 10 nm increments. It was found that the peak in the light source spectrum shifts drastically as this was done, as can be seen in figure 28.

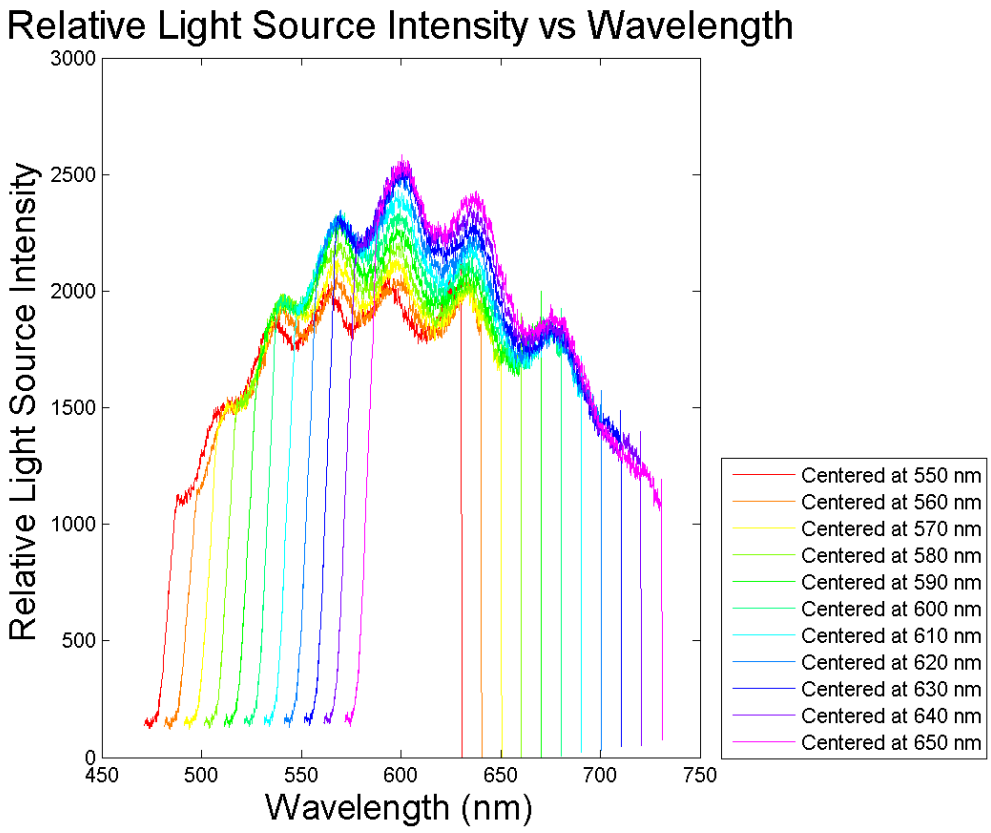

Figure 29: Light source spectrum measured as the spectrometer window is moved after using the fiber alignment tool

The problem of the shifting spectrum as the center of the spectrometer measurement window is shifted was corrected by using a fiber alignment tool. The alignment tool allows the fiber at the entrance slit of the spectrometer to translate on the X and Y axis as well as tilt so as to align the fiber normal to the entrance slit. Figure 29 shows the result of repeating the test after using the fiber alignment tool. The peaks in spectrum no longer shift as the center wavelength of the spectrometer window is moved with the exception of the window centered at 550 nm.

Repeatability of Measurements

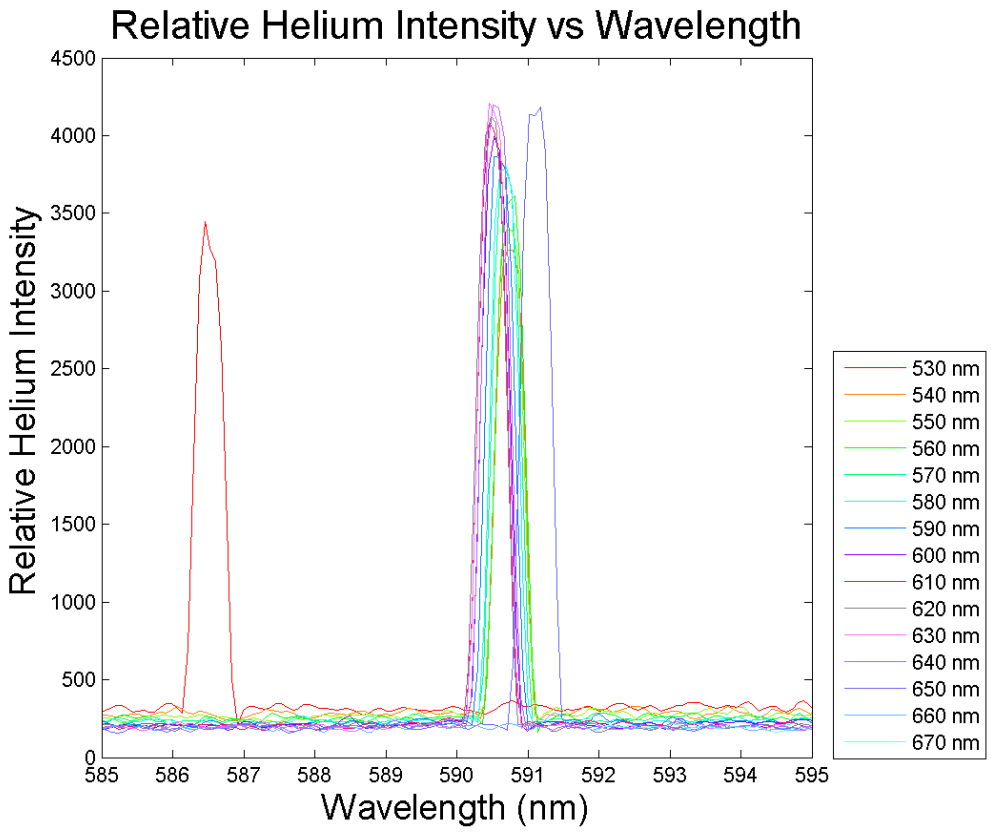

Figure 30: A Peak of the helium spectrum as the spectrometer window is moved incrementally by 10 nm.

Although the fiber alignment corrected most of the shift in the spectrum as the spectrometer window was shifted, the spectrum from the window centered at 550 nm still shifted. It was decided to repeat the test of using Helium Spectrum instead of the light source to see how repeatable this error from the spectrometer was. Figure 30 shows a single peak of the Helium spectrum from that test. It was found that although the peak generally did not move, it did shift when the window was centered at 530 and 670 nm.

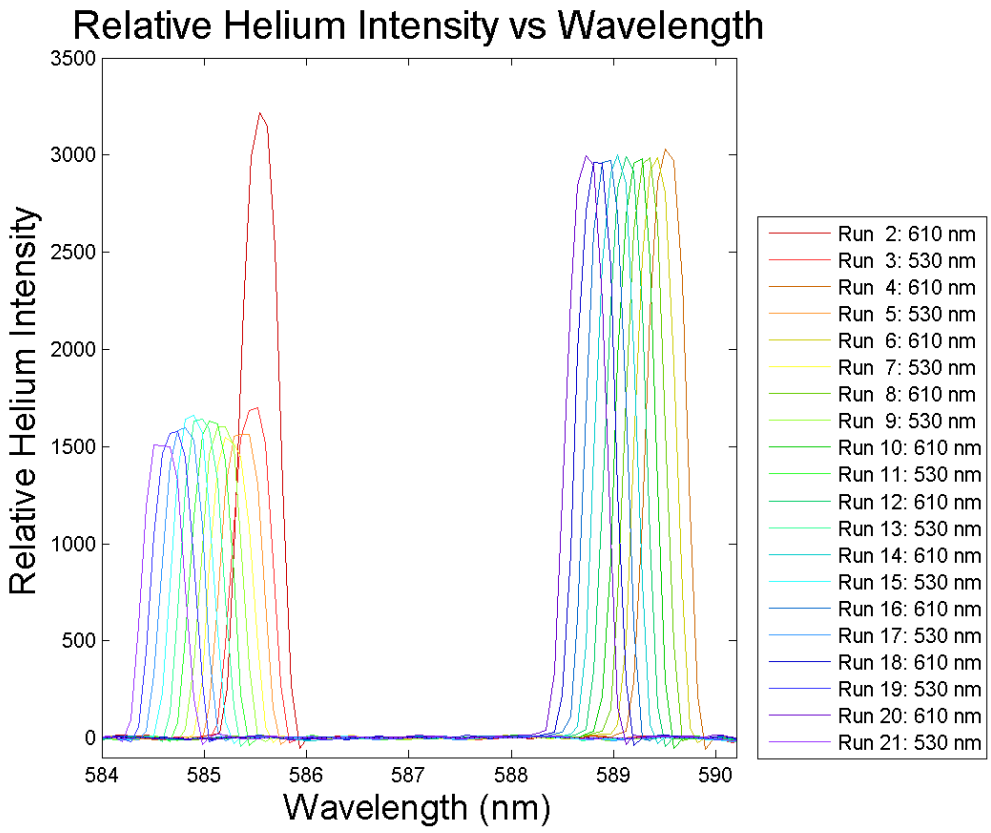

Figure 31: Repeatability test of helium spectrum lines by moving the spectrometer window between being centered at 530 and 610 nm repeatedly

The spectrum shifting as the spectrometer window is shifted could potentially be corrected by calibration as long as the shifting is consistent. To see how consistent or repeatable these shifts in the spectrum were the spectrometer window was repeatedly moved between being centered at 530 nm and 610 nm while measuring the helium spectrum. Figure 31 shows a single helium peak from that test measured from each spectrometer window. It was found that the first 610 nm window is located next to all the peaks with the spectrometer window centered at 530 nm.

The figure shows that the peak from the first 610 nm window is located next to all the peaks from the 530 nm windows and that every time that the window is shifted the

peak is also shifting ever so slightly. Over time, this quickly adds up and exceeds the manufacture's repeatability specification of less than 0.1 nm [12]. This repeatability problem can be overcome by calibrating the spectrometer window at the beginning of a test and not moving its location until the test is finished. It was decided to investigate whether or not the calibrated spectrometer window was broad enough to capture all of the crystal response.

Wavelength Calibration

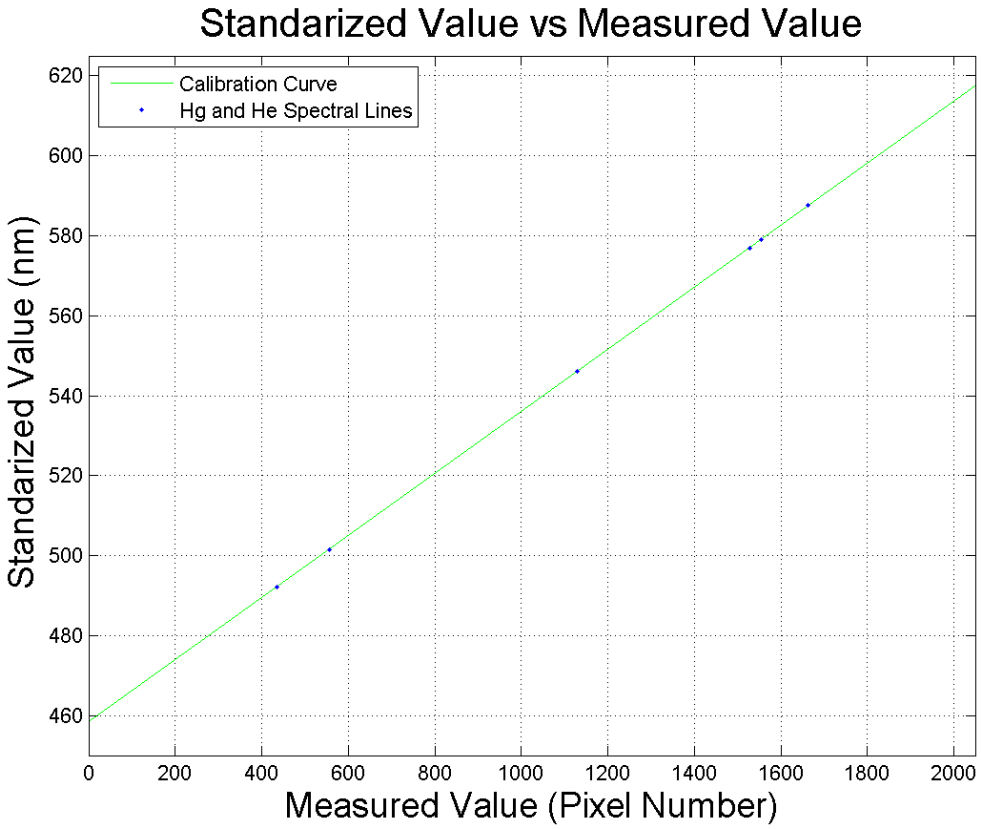

Figure 32: Calibration Curve for the spectrometer window centered at 535 nm

The spectrum of helium and mercury were measured and then the peaks were fit with Gaussian curves. The mean values of each peak were then plotted with known values of a peak [13] on one axis and the measured value on the other. These points were then

used to produce a calibration curve by fitting a straight line which can be seen in figure 32.

Combining Multiple Windows

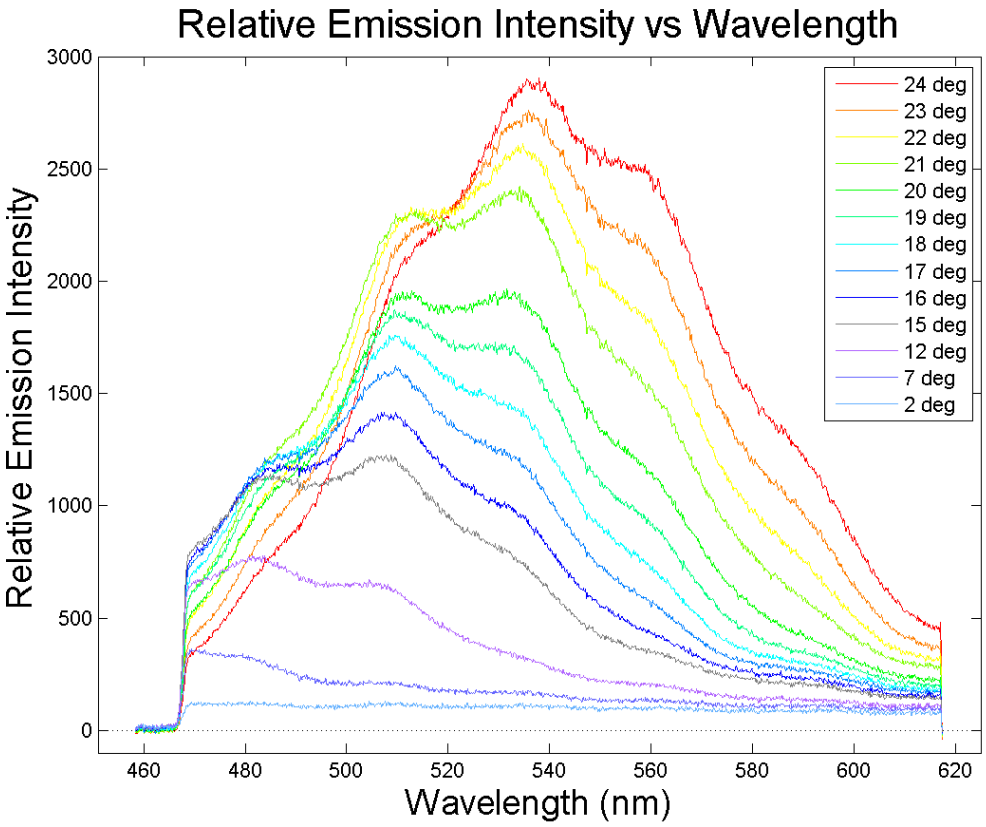

Figure 33: Crystal response as theta is varied using a single spectrometer window

The first set of measurements used the initial stand design that allowed for the rotated theta with the light source and collection fiber being separate as shown in figure 33. This test shows that the spectrum of the crystal shifts enough that part of the spectrum leaves the measurement window. This requires a larger measurement window or for multiple windows to be combined to see the full crystal response as the theta is varied.

Using multiple measurement windows requires that the spectrometer be recalibrated every time the window is moved because of the repeatability problem. However, the amount of measurements needed makes this time consuming and unpractical. It was decided that since the spectrum of each measurement was to be converted to a color value it could be assumed that the auto-calibration feature of the spectrometer could be used.

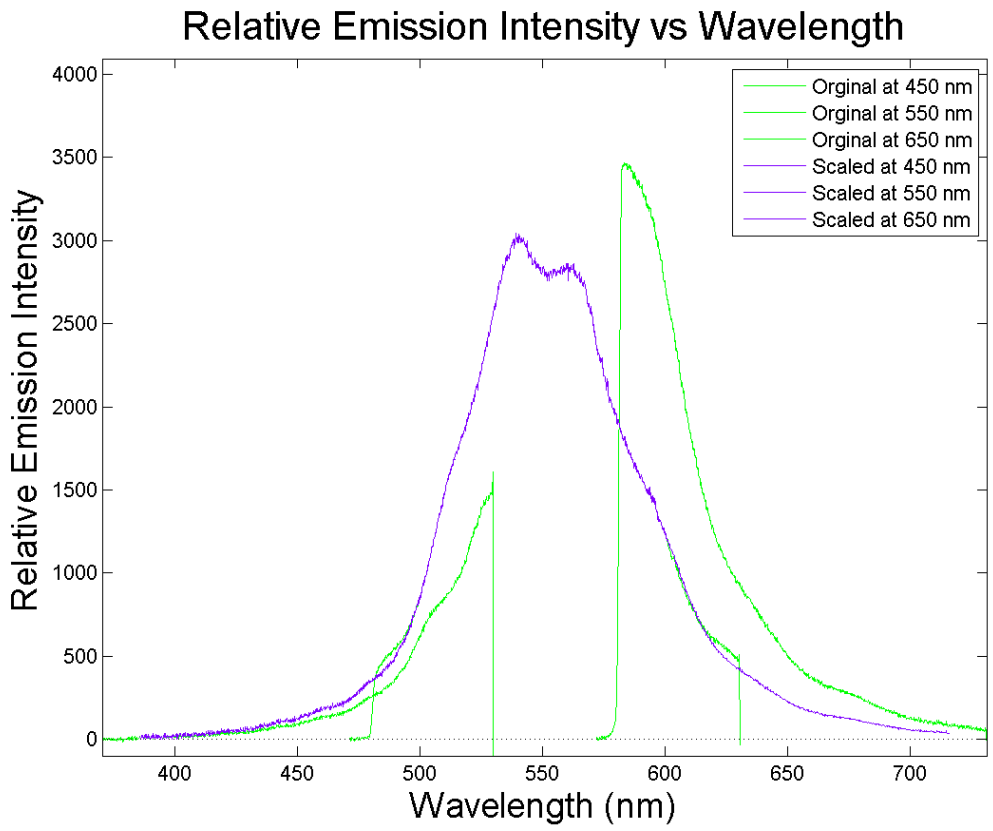

Figure 34: A set of three overlapping spectrometer measurement windows measuring the crystal response were taken and then combined. The before and after results are shown

A set of three overlapping windows measuring the crystal response were taken to test combining three windows centered at 450, 550 and 650 nm. Before the windows were combined, 15 nm on the edges of each window were cut off due to edges not

functioning as well and can be seen in figure 33. In order to combine each window with another one, an overlapping wavelength was picked for transitioning from one window to another. The transition points are located at 500 and 600 nm. The spectrum of the lower window is then cut off above the transition point as well as the spectrum of the higher window below the transition point.

Due to different efficiencies of the detectors in the spectrometer for different wavelengths of light, the overlapping intensities differ by up to 3 or 4 times the other value. The lower and higher windows were normalized to the center window to overcome this. This was done by scaling the windows by a scaling factor determined by the ratio of the average of 10 values at the transitioning point of the lower and higher window. Figure 34 shows the before and after from combining the three windows from a single spectrum of a crystal response.

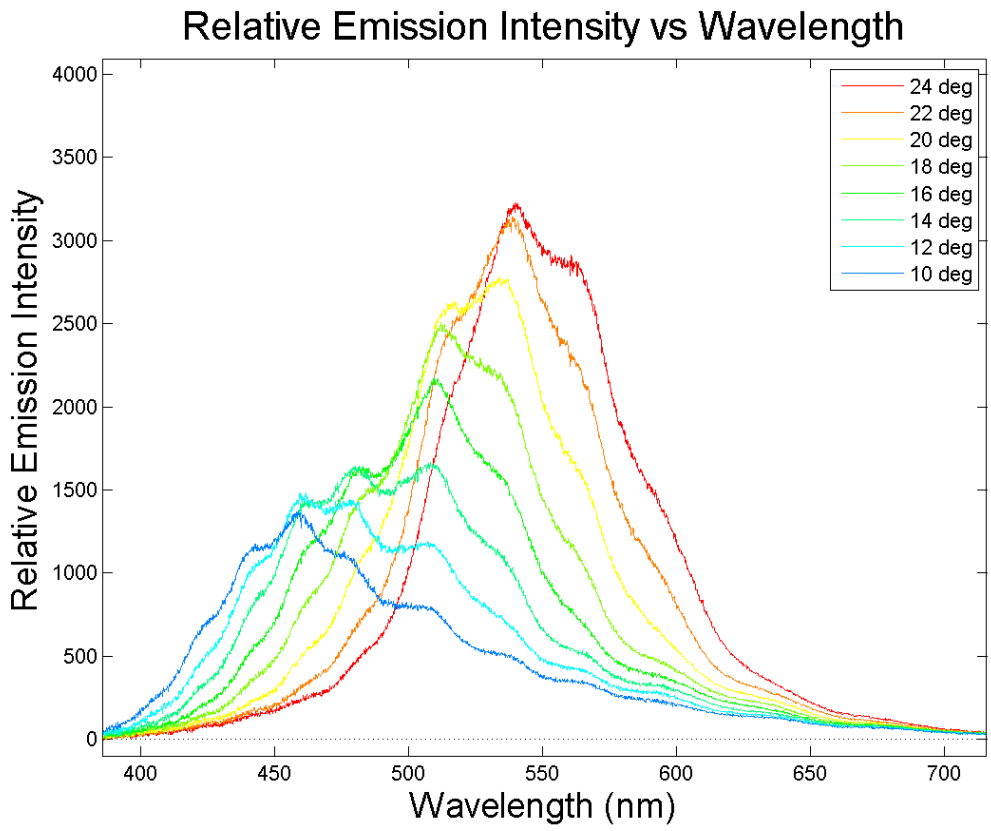

Figure 35: The spectra of the crystal response as theta is varied using three measurement windows combined together

The earlier test shown in figure 33 was repeated using three overlapping spectrometer measurement windows at each theta location instead of a single window. The three measurement windows at each sampling location were centered at 450, 550 and 650 nm. The spectrums from each sample location were combined as described above and plotted as shown in figure 35. This shows that these three windows cover most of the crystal response and that the response does not leave the measurement window. The measurement window also more closely aligns with the range of the color matching function which allows for better color conversion values.

Experimental Procedure

The experimental procedure measures the crystal response spectrum at various locations surrounding the photonic crystal by varying theta and phi. Theta and phi locations are not measured at all angles because the crystal response is assumed to be symmetrical. Theta is measured between 0 and 90 degrees while phi is measured between 0 and 45 degrees. The second test stand setup was used which used the collinear light source and fiber collection point. The fiber going into the spectrometer is aligned before the test if it has not been done previously.

The first step is to mount the sample with the photonic crystal to the XRD stand using carbon tape and then adjust the position of the crystal so that it is at the center of the fiber rotation which coincides with the eucentric height of the stand. This is done by first rotating the crystal to approximately normal to the viewing optics piece of the stand and adjusting the height of the sample to the focus of the optic piece. The crystal is then translated on the x and y-axis to the center of the viewing optics. The sample is then rotated back and forth to check if the position of the crystal changes. If the position changes, the height and XY position is adjusted until the crystal no longer changes position as the sample is rotated back and forth.

Once the crystal has been placed in the center of the fiber rotation, the fiber needs to be positioned where it can collect the crystal response with the greatest intensity for a particular theta and phi position. Typically the theta position with the highest intensity of the crystal response with phi fixed to zero is picked to determine the fiber position.

The test stand fiber rotation arm can translate the fiber on its x, y and z axis's which allow for the best placement of the fiber. The fiber is translated on the z-axis to be the greatest distance away from the crystal and still collect a good signal. The exposure time of the spectrometer can be increased to increase the distance of the fiber from the crystal. The x and y position of the fiber is moved to where it will receive the greatest intensity of crystal response.

Measurements of the crystal response are taken in 5 deg increment while varying theta and Phi. The first initial measurements are taken by varying theta from 50 to 15 degrees while phi is fixed to zero degrees. Theta cannot extend beyond 50 degrees due to physical limitations of the fiber contacting the sample. Theta also cannot extend below 15 degree due to oversaturation of the spectrometer from the reflection of the light source. After this cycle of measurements is completed the crystal is then translated in the x y plane so that it is moved out of the spot of light. A background reading is now taken by repeating the measurements in the reverse order.

The next set of measurements fixes theta to an angle and varies phi. Phi is varied by rotating the crystal from 0 to 45 degrees in 5 degree increments. At each phi location, a background reading is made by moving the crystal out of the spot of light by translating the crystal in the x and y plane. The crystal is then translated back into position after the reading. The crystal moves from the center of the fiber rotation each time the crystal is rotated in the x y plane. The x y adjustment on the stand is then used to bring

the crystal back to the center of the fiber rotation each time the crystal is rotated.

These steps are used for each desired theta location while varying phi as desired.

Analysis and Results

Initial Results

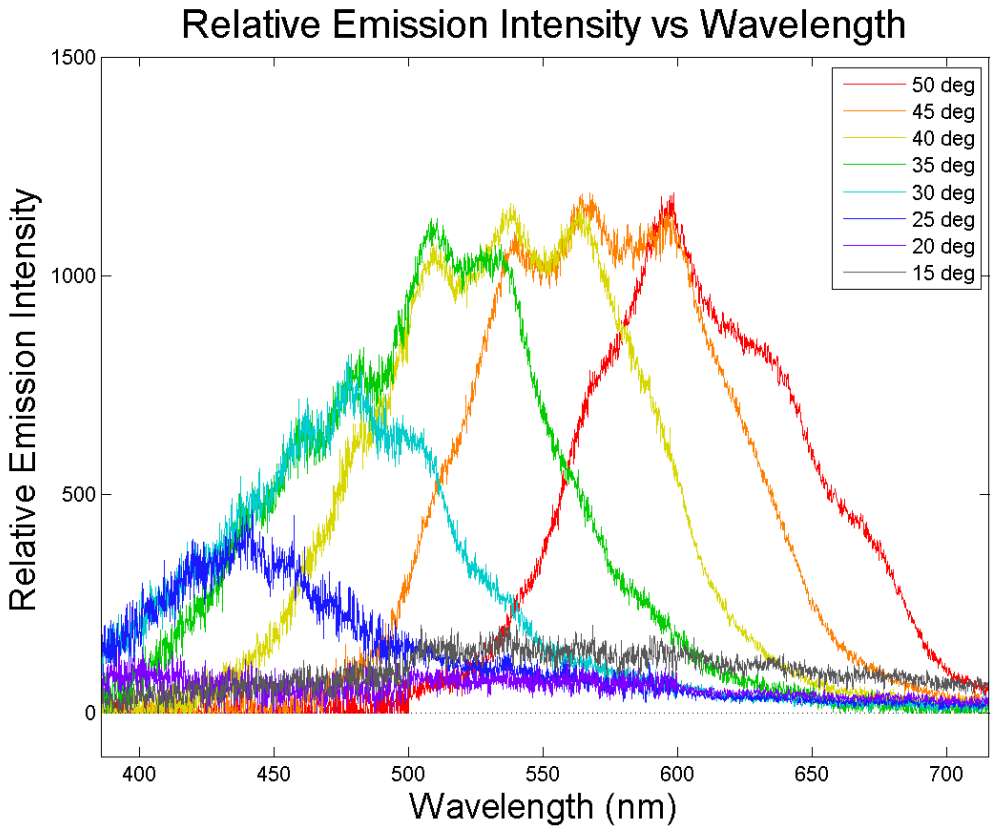

Figure 36: Initial test using the final test stand setup and only varying theta

The first initial test using the final test stand setup only varied theta while phi was fixed at 0 degrees. Any negative values resulting from subtracting the background are made to equal zero since there cannot be a negative reading of light. The results show many peaks in the spectrum as can be seen in figure 36. It was decided to investigate whether this could be the result of the shape of the light spectrum since the crystal response would increase at wavelengths of higher intensity of the light source

spectrum. This was done by taking a ratio of the spectrum from the crystal response and the light source.

Crystal Response / Light Source Spectrum

Smoothing

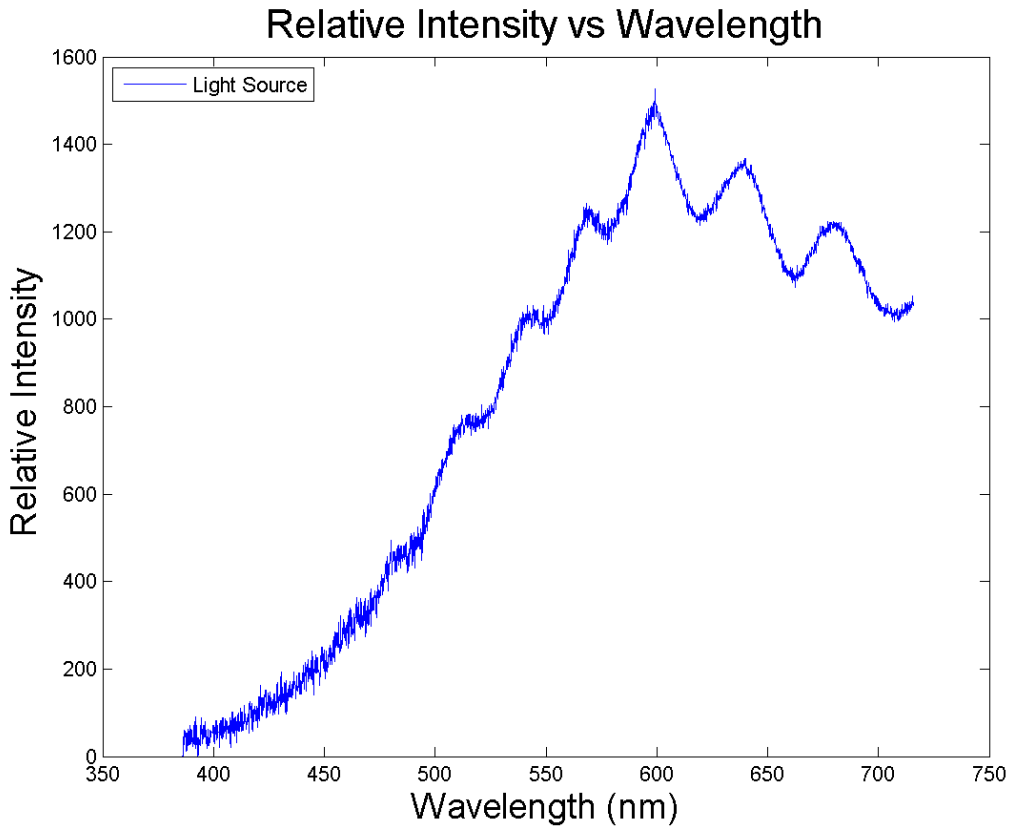

Figure 37: Light source used to produce the crystal response

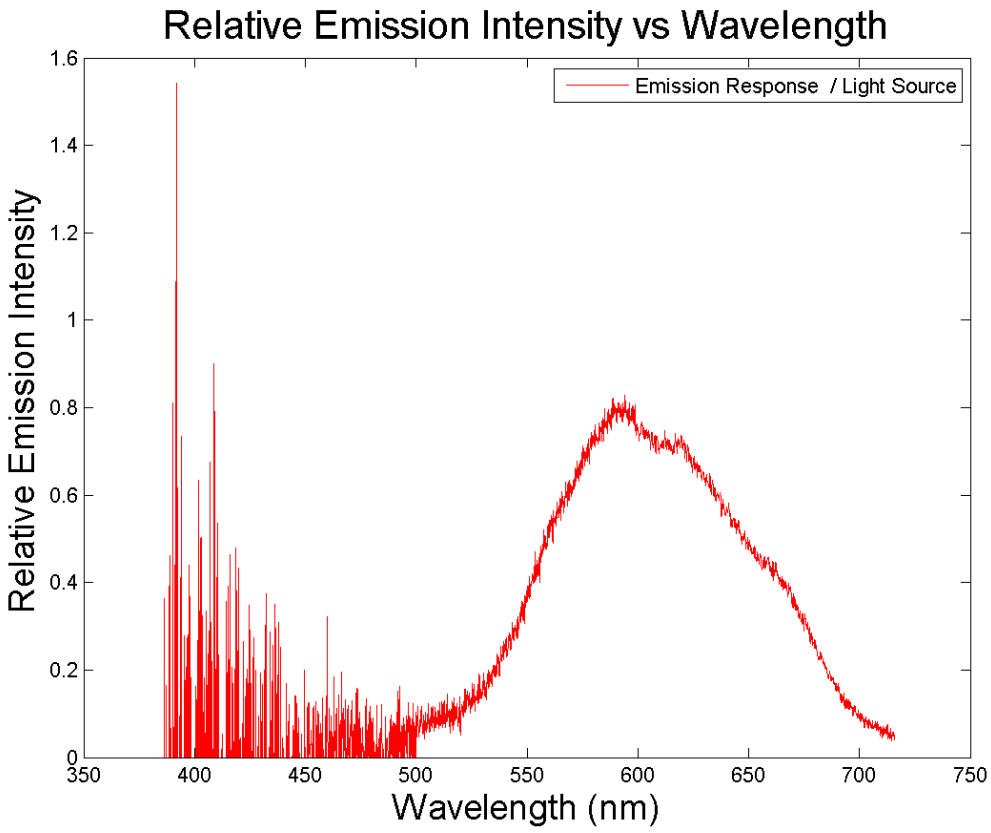

Figure 38: The spectrum of the crystal response at theta of 50 degrees divided by the spectrum of the light source

The first attempt to divide the crystal response by the spectrum of the light source was tested on the spectrum from the location where theta equals 50 degrees, and phi equals 0 degrees. Figure 37 show the spectrum of the light source used to produce the crystal response. The division of the crystal response and light source resulted in a spectrum where most of the small peaks have been removed from the spectrum leaving one big peak as shown in figure 38. However, it also resulted in high-intensity values at the lower wavelengths. This is from the light spectrum and crystal response both having low intensities in the region allowing the noise to wreaked havoc on the resulting spectrum.

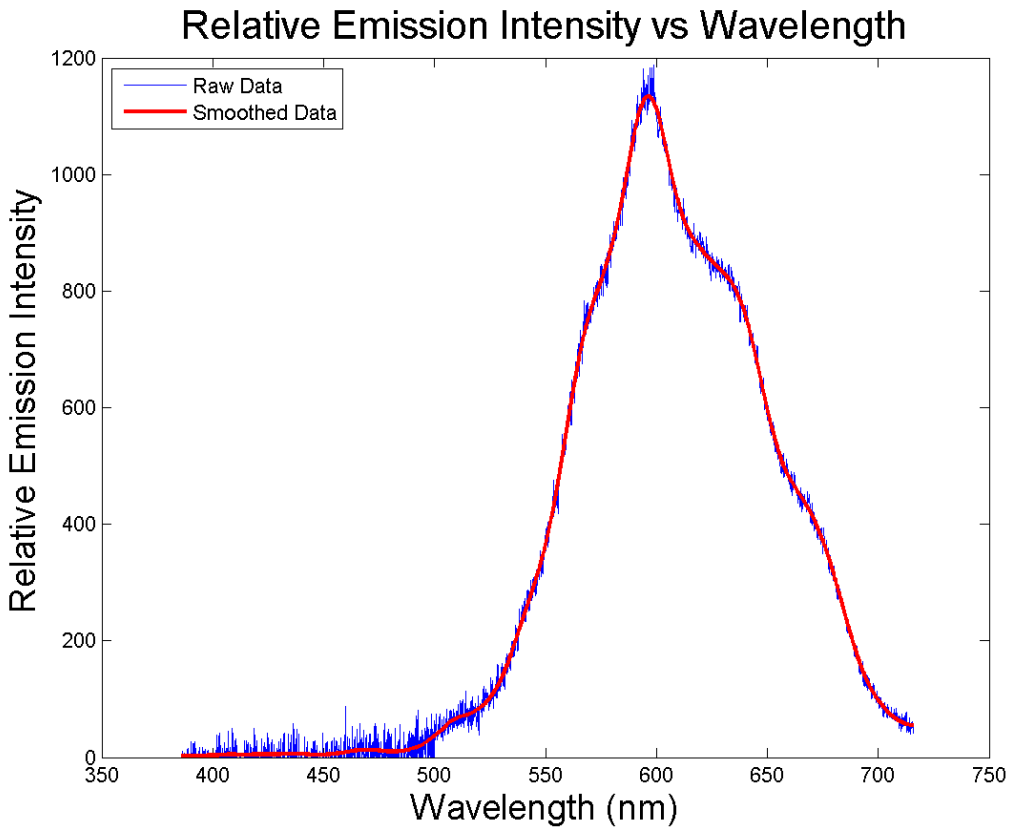

Figure 39: Smoothed and raw data of the crystal response at theta of 50 degrees

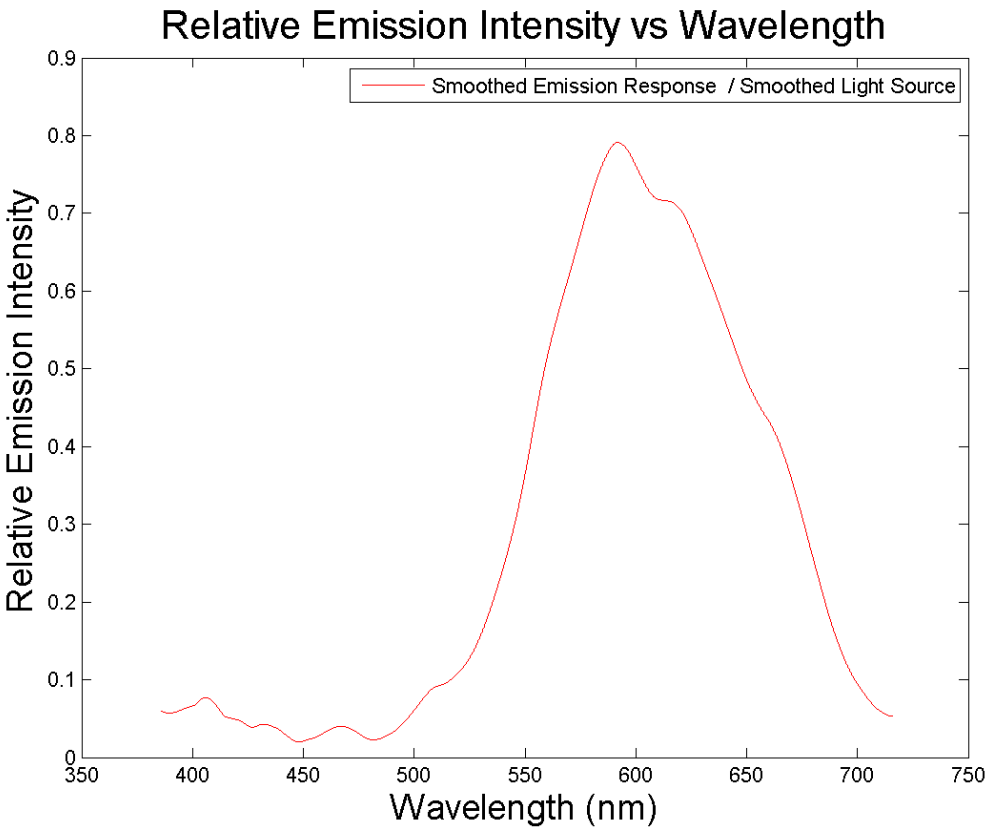

Figure 40: The crystal response at theta of 50 degrees divided by the light Source after smoothing

The spectra of both the light source and crystal response were smoothed to remove the noise produced by the division of the two spectra. The smoothing was accomplished using a LOESS algorithm. The smoothed spectrum of the crystal response at theta of 50 degrees and phi of 0 degrees is shown in figure 39. The division of the smoothed crystal response by the smoothed light source data is shown in figure 40. The result of the smoothing operation shows that high-intensity values at the lower wavelength no longer exist.

Crystal Response / Light Source Spectrum

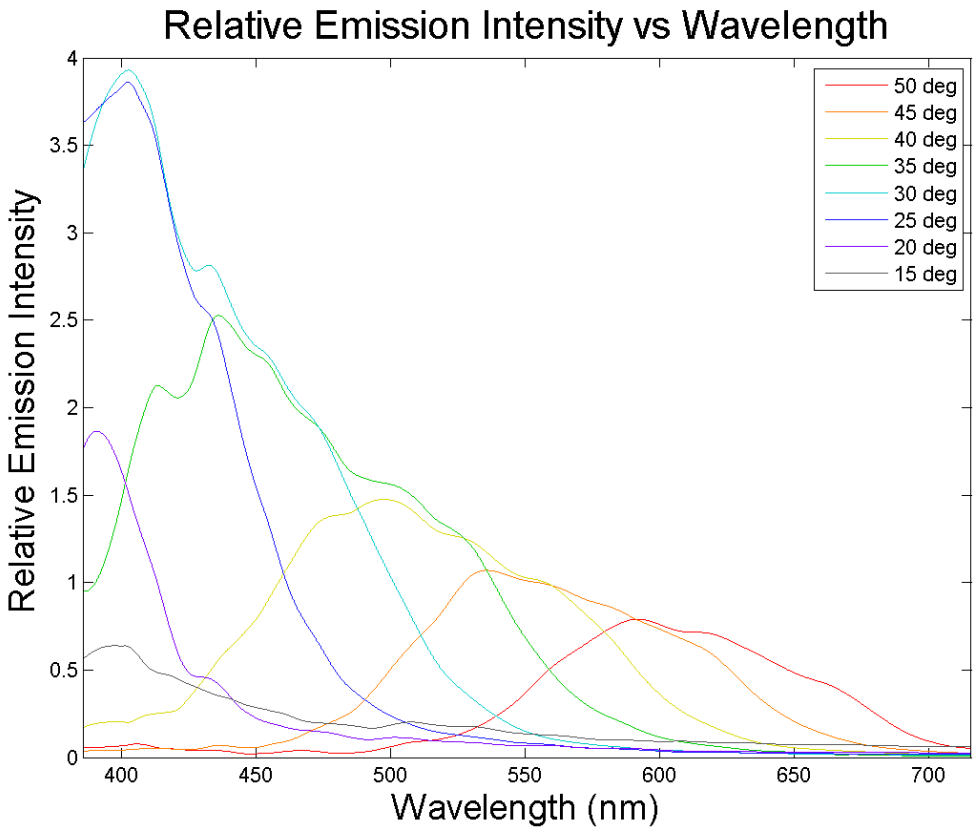

Figure 41: Spectra of the crystal response from the entire initial test divided by the spectrum of the light source after smoothing

After testing the division of the smoothed crystal response and smoothed light source on the spectrum from one location, the method was expanded to all locations of theta as shown in figure 41. It was found that the intensity of the spectrum greatly increased from theta of 40 degrees to 20 degrees which was unexpected. Further investigation of this effect follows below.

Remove Scaling

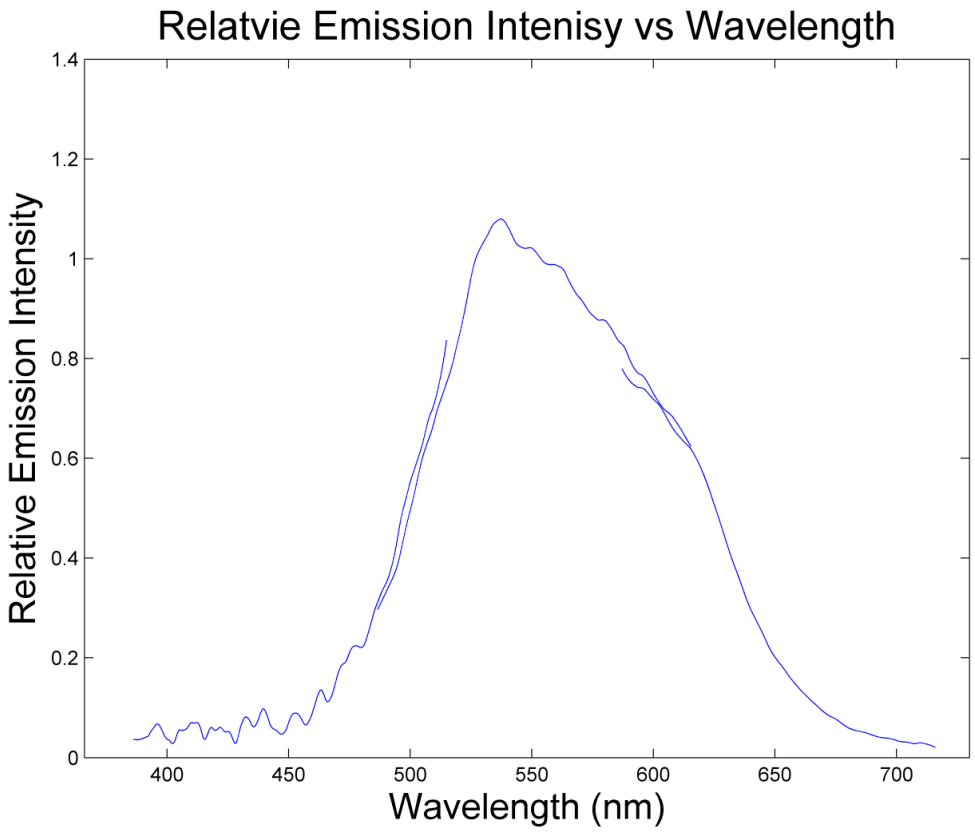

Figure 42: Spectrum of crystal response at theta of 45 degrees divided by the spectrum of the light source without scaling and combining of the spectrometer measurement windows

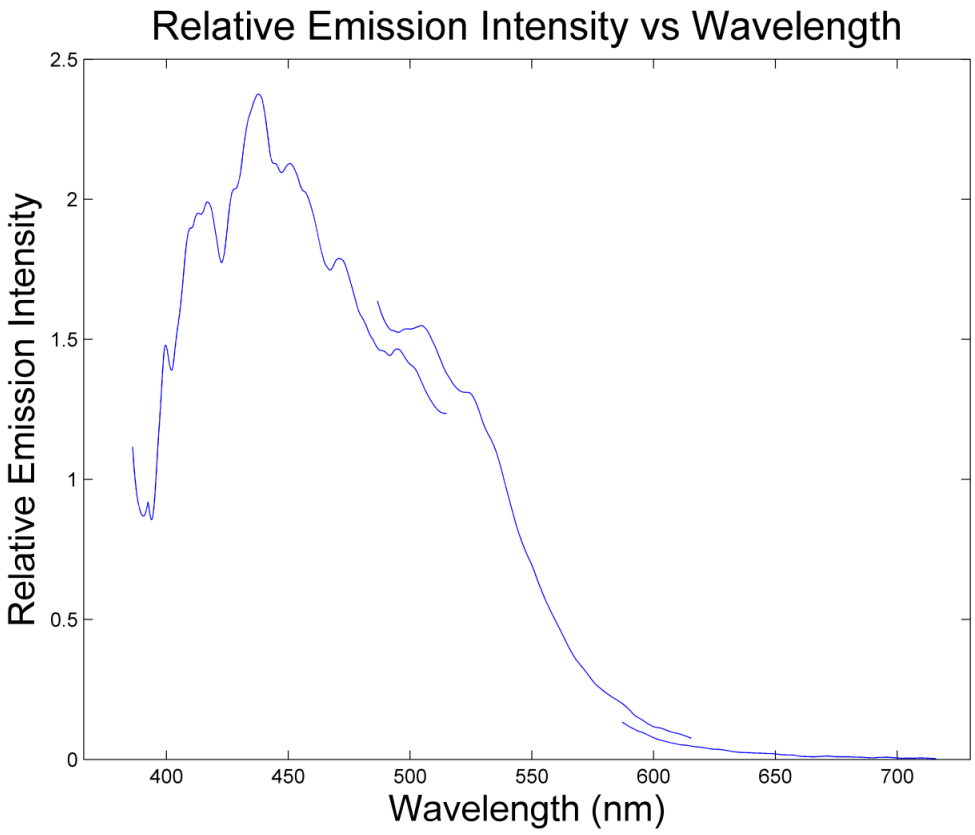

Figure 43: Spectrum of crystal response at theta of 35 degrees divided by the spectrum of the light source without scaling and combining of the spectrometer measurement windows

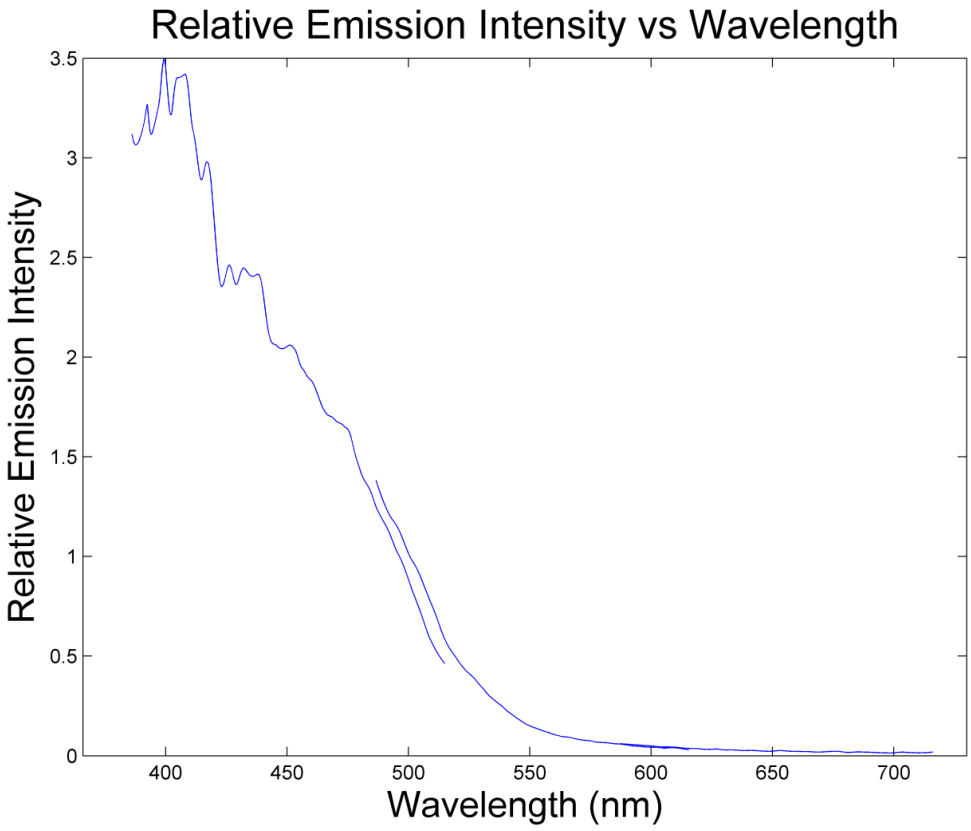

Figure 44: Spectrum of crystal response at theta of 30 degrees divided by the spectrum of the light source without scaling and combining of the spectrometer measurement windows

One of the first things investigated was how the scaling to combine three windows might affect the result of the division of the crystal response and light source. This is because the higher and lower windows are scaled by a factor of up to 3 or 4. However, since the spectrum of the light source and crystal response are scaled similarly, the scaling factor effectively cancels each other out. Even though scaling factors are approximately the same, the scaling factor can be slightly different producing a slight alteration of the resulting division. To remove this effect, the division was applied to all three windows separately without combining them and then plotted together as can be seen in figures 42, 43 and 44.

Crystal Response / Reflection of Light Source on Steel

Light Source / Reflection of Light Source on Steel

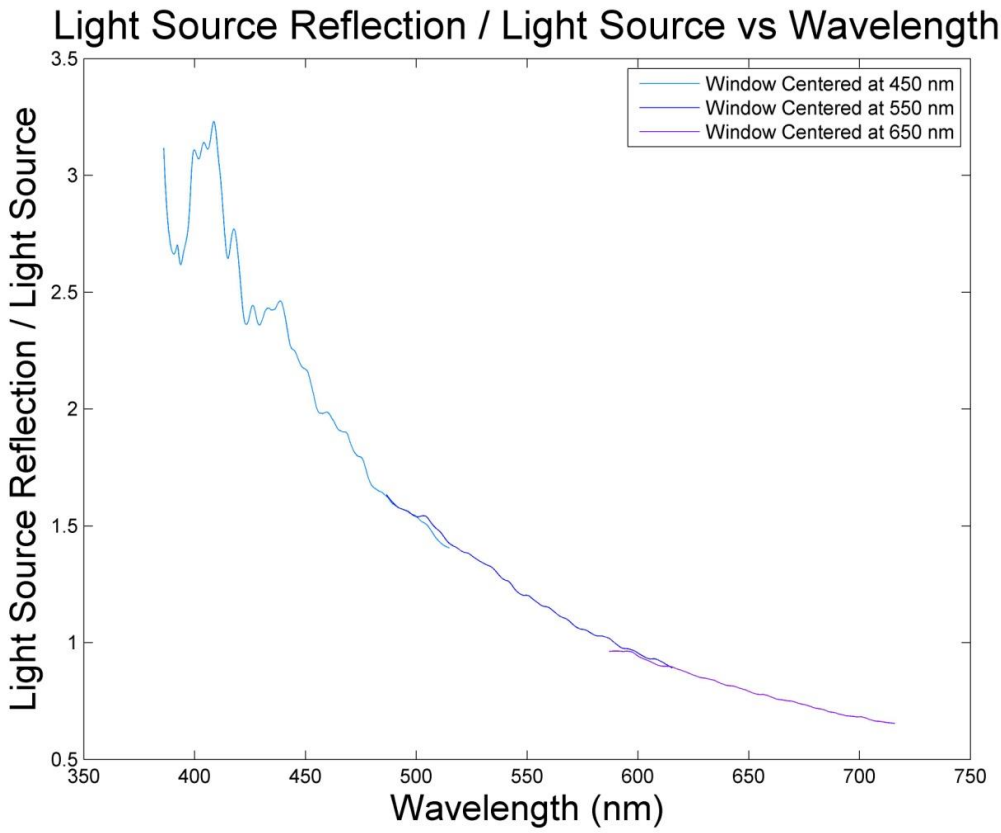

Figure 45: Spectrum of the light source divided by the reflection of the light source on the surface of steel

The possibility that the coloration of the steel affected the crystal response was investigated by dividing the spectrum of the light source with the spectrum of the light source reflected from the surface of steel. A perfect reflection of the light source on the steel would result in a horizontal line parallel to the x-axis from the division of the two spectrums. During the measurement of the reflection of the light source, the light source, and the collection fiber were collinear and positioned normal to the surface of the steel. The spectra of the reflected light source on steel were measured at seven locations on two samples of steel to understand how the surface at each of the different

locations could affect the light source spectrum differently. Figure 45 shows the result of the division of the light source by the reflection of the light source on steel for one of the locations the reflection was measured. It can be seen that the coloration of the steel does indeed affect the spectrum of the light source in the region of lower wavelengths. It was also found that the spectrum from each location has a similarly shaped spectrum but differ a little by the intensity.

Crystal Response of the Initial Test / Reflection of Light Source on Steel

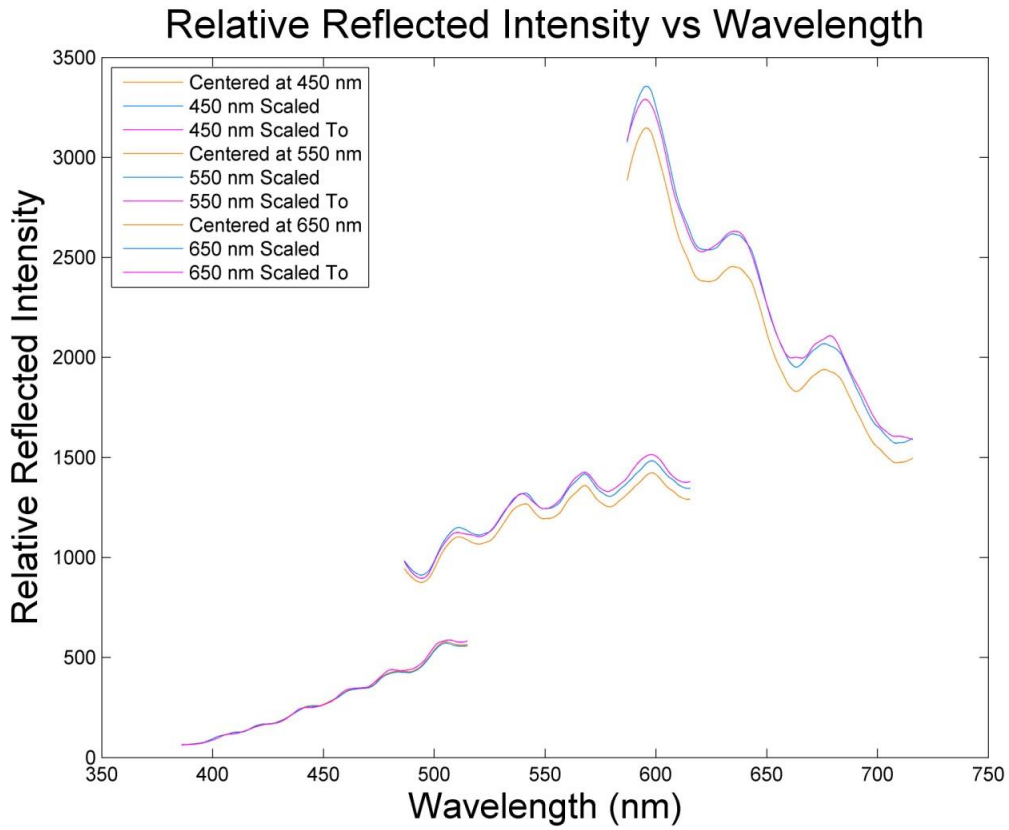

Figure 46: Shows the spectra of the reflected light source spectrum from sample 1 location 2 before and after the normalization with the spectra they are normalized to

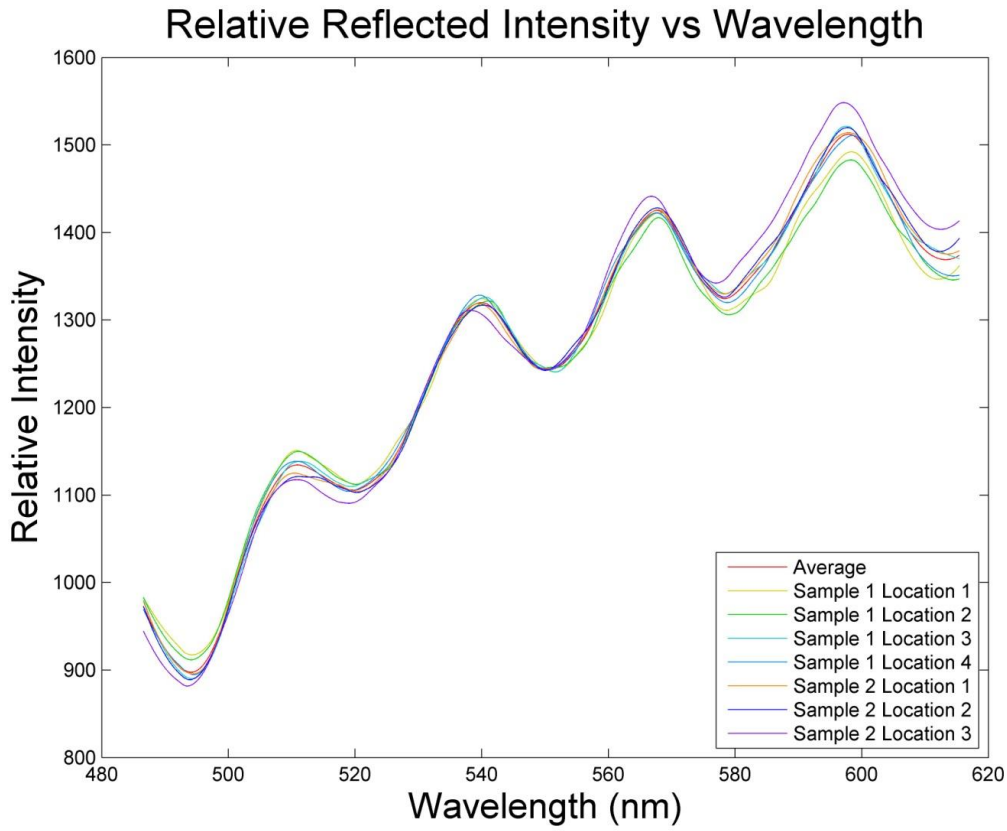

Figure 47: The normalized spectra of the light source reflection on steel at all 7 locations on 2 samples and their average for the center measurement window

The spectra from the reflection of the light source on steel at the seven locations were averaged together and then the crystal response was divided by that averaged reflection spectrum. The reflection was measured at different locations and then averaged to minimize any effect of surface anomalies at any one location in the reflection of the light source. To ensure that no one spectrum would bias the average, the spectrum from each location was normalized to the spectrum of a single location before averaging them. It was desired that this normalization would effectively make each reflection section weighted equally. The spectrum from each location was normalized by scaling it using a ratio of the averaged of values at the center of its

spectrum and that of the location spectrum it was being scaled to. Figure 46 shows the before and after of normalization along with the spectrum it was normalized to. Figure 47 shows the spectrum of each location after normalization and the average of all the spectra for the center measurement window.

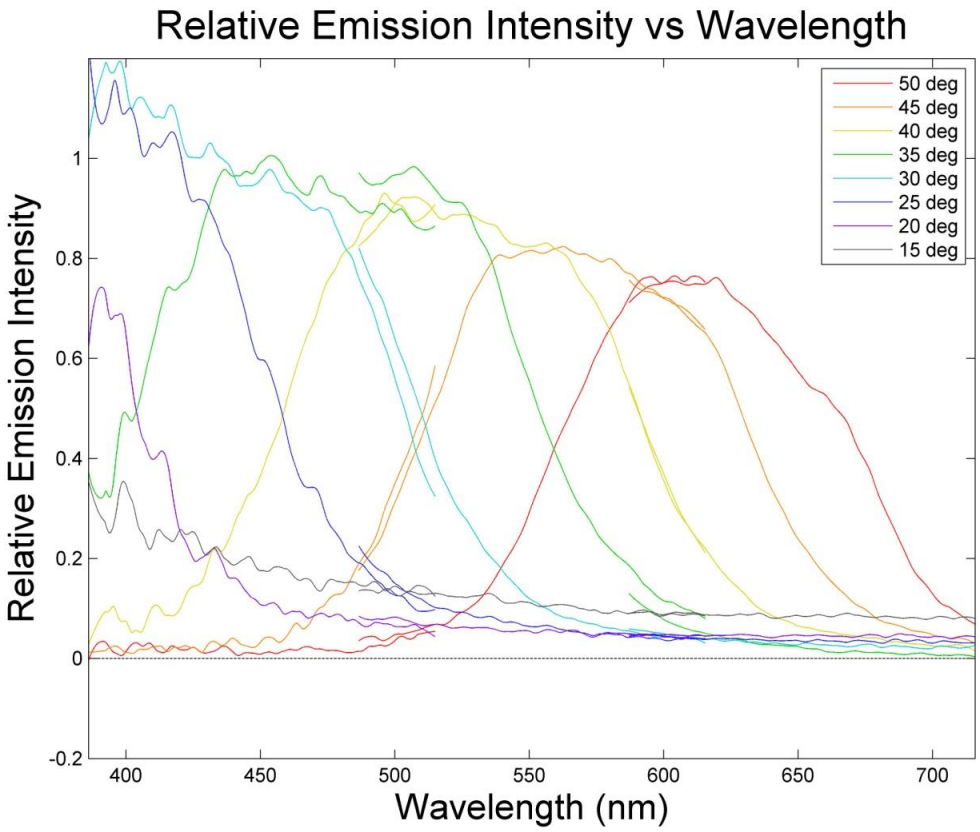

Figure 48: Crystal response at each sampling location is divided by the reflection of the light source on steel

The crystal response of the initial test was then divided by the average reflection of the light source on steel to remove the coloration effect of the steel. The result is shown in figure 48. It can be seen from the figure that the lower wavelengths are no longer much larger than the rest of the sample locations of theta.

Crystal Response of the Full Test / Reflection of Light Source on Steel

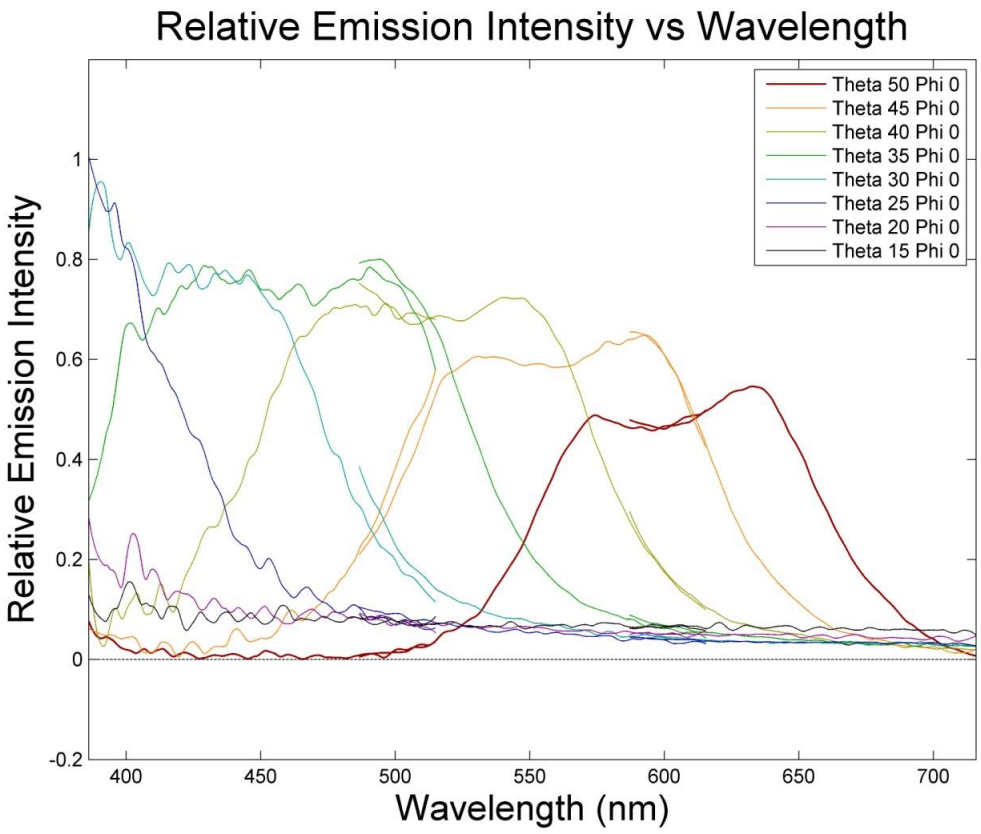

Figure 49: Final test at phi of 0 degrees while theta is varied

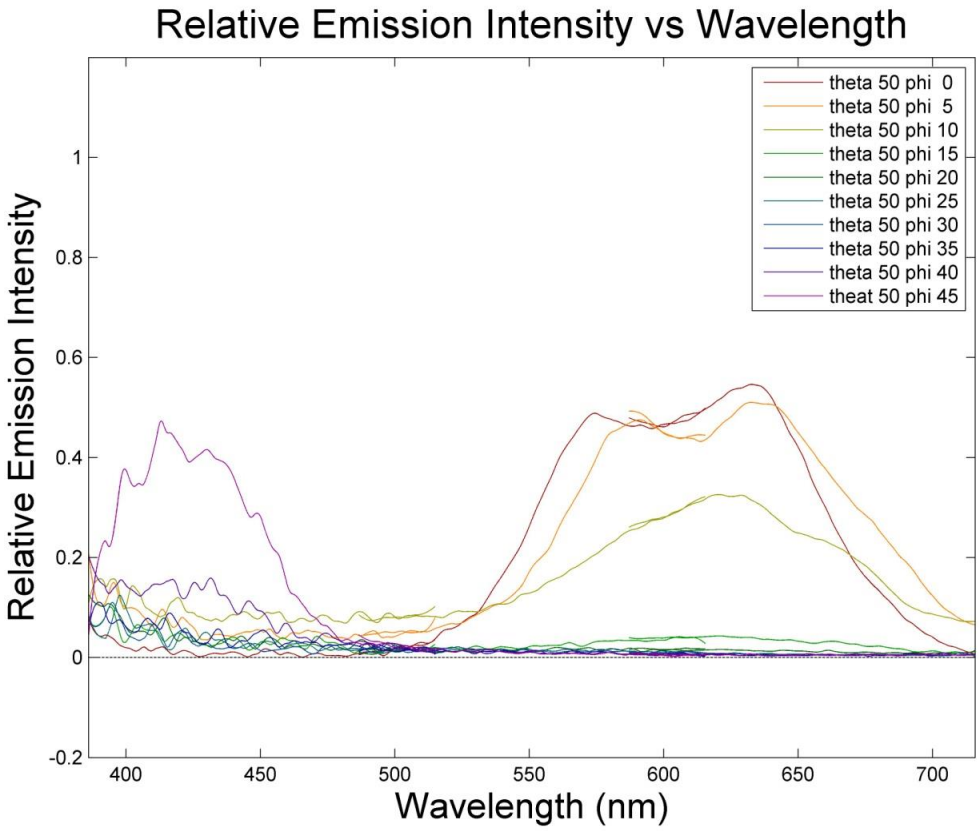

Figure 50: Final test at theta of 50 degrees while phi is varied

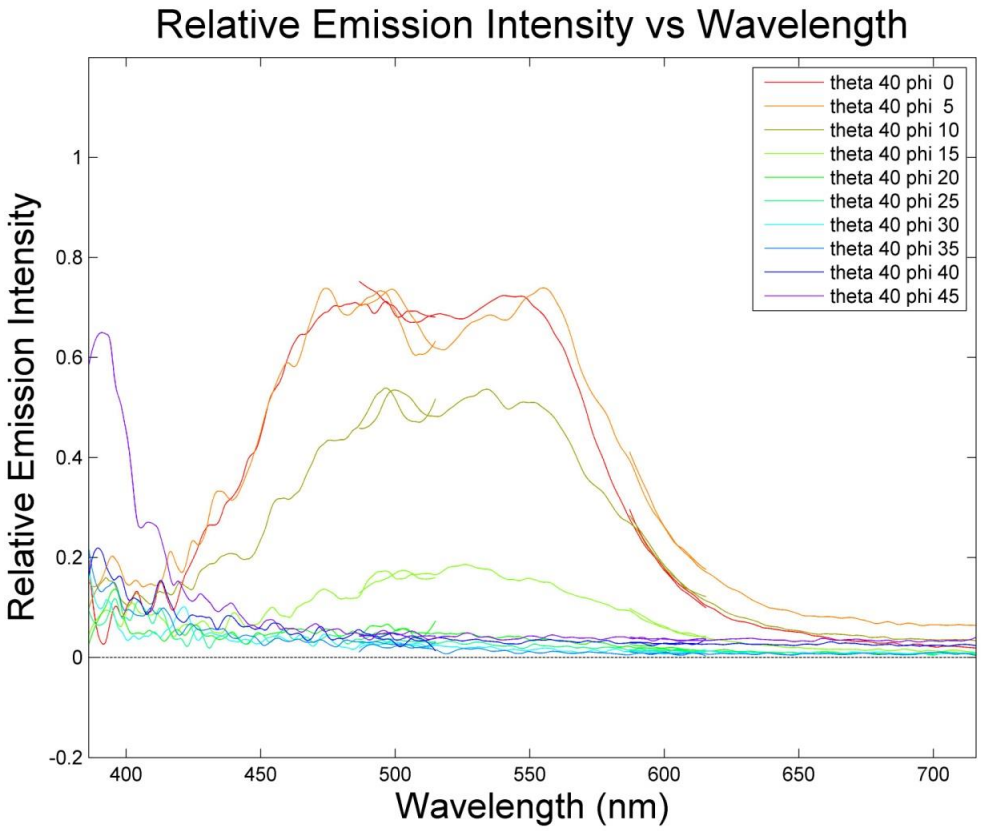

Figure 51: Final test at theta of 40 degrees while phi is varied

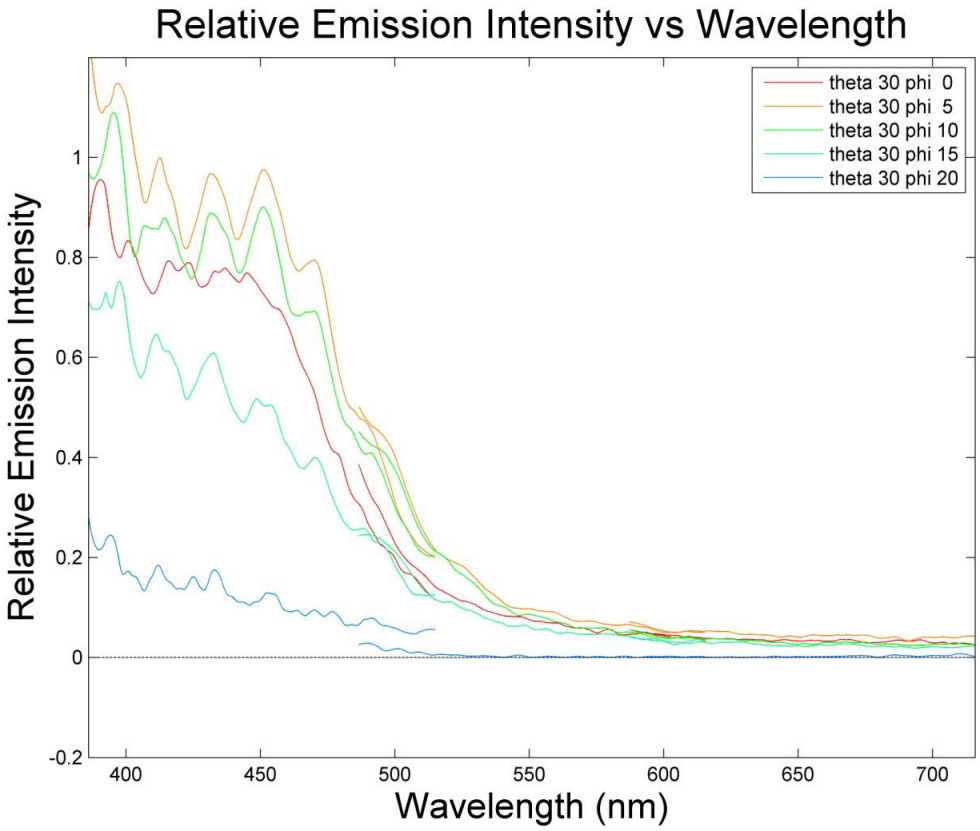

Figure 52: Final test at theta of 30 degrees while phi is varied

The full test as explained using the experimental procedures was completed after completing the removal of the coloration effect on the initial test. This test differs from the initial test by sampling the crystal response by varying both theta and phi instead of only theta. The full test samples a limited number of locations but still demonstrates the use of the stand. Figures 49 through 52 show the results of the full test with the crystal response divided by the reflection of the light source on steel. Figures 49 show the result of theta being varied while phi was fixed to 0. Figures 50 through 52 show the result of Phi being varied at three different locations of theta.

Color Analysis

Purpose of Color Plot

The spectrum of the crystal response at each location is converted to a color and used to create a color plot. A color plot is a quick visual synopsis of the crystal response at each sample location. Further investigation is then required by then looking directly at the spectrums of the crystal response at points of interest. The process of converting the spectrum of a crystal response is explained in the following sections below.

CIE 1931 Color Matching Function

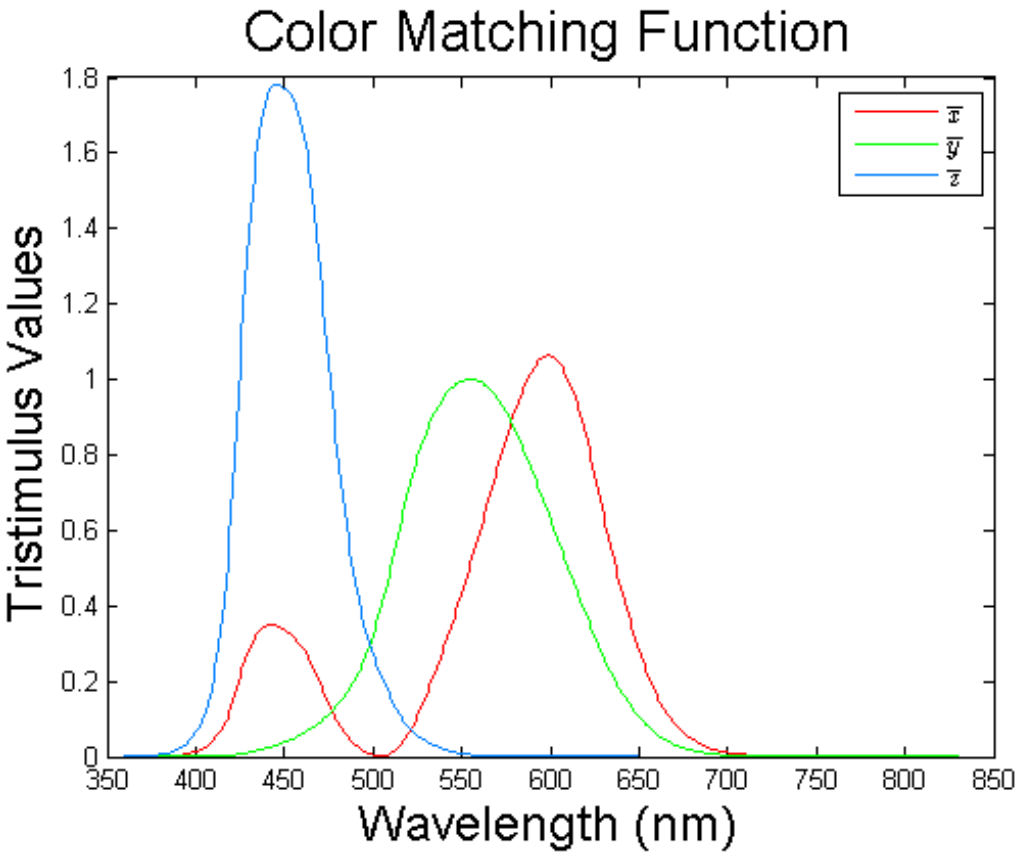

Figure 53: CIE 1931 color matching functions. This plot was created using color matching function values found in Wyszeck and Stiles' *Color Science* [14]

Color stimuli can be created by an additive mixture of three primary stimuli. Color stimuli are represented in 3D space by using vectors called tristimulus space [14]. The tristimulus values are determined by weighting the spectrum of the crystal response by color matching functions [14]. The CIE 1931 color matching function was used to determine the X, Y and Z tristimulus values for the spectrum of each crystal response [14]. The tristimulus values are then bound between 0 and 1 before converting the values to another color gamut that is used by the plotting program. This is accomplished by normalizing them to XYZ tristimulus values of a spectrum with constant values of a desired max intensity.

Converting the Spectrum to sRGB Values

The XYZ tristimulus values of the CIE 1931 gamut were converted to the sRGB gamut for compatibility with the plotting program. sRGB is a color gamut that is used on monitors and printers [15]. The conversion is accomplished by using a transformation matrix and gamma correction from the IEC 61966-2-1:1999 standar [16]. Once the sRGB values are obtained, they are converted from a 0 to 1 range to 8 bits by multiplying by the values by 255 and rounding to the nearest integer.

Color Plot

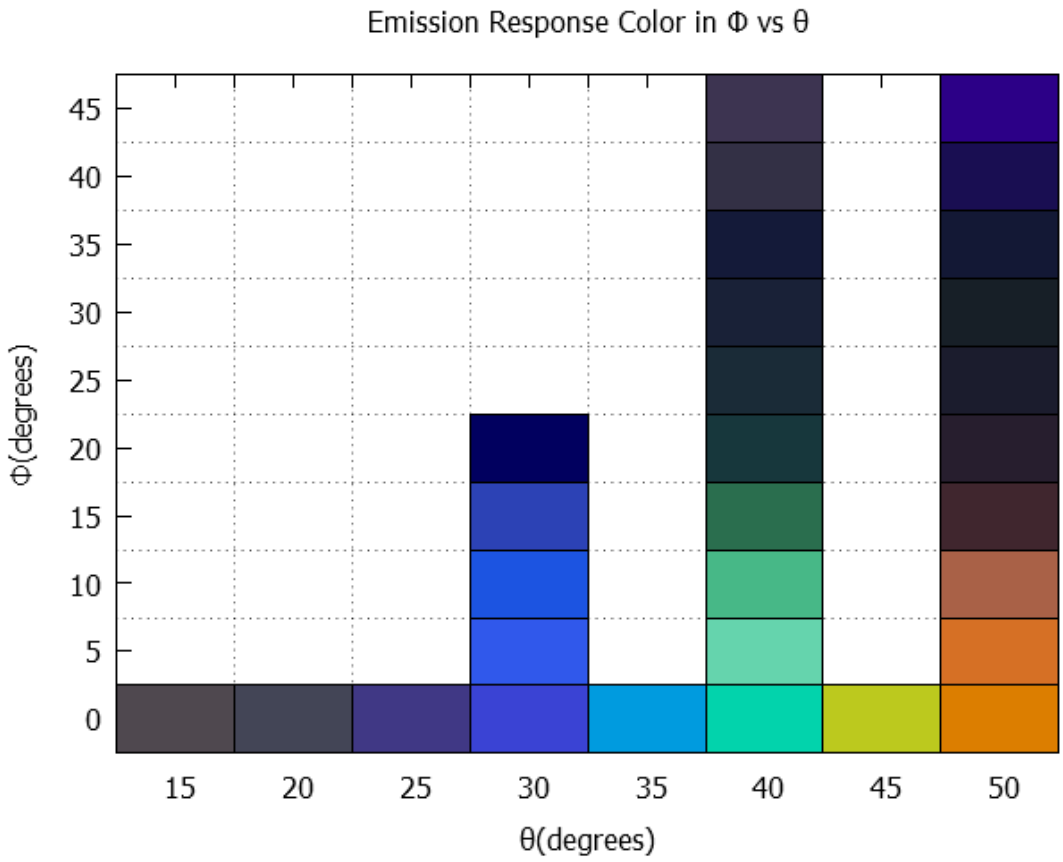

Figure 54: Color plot of the crystal response. Each square represents a sampling location specified by theta and phi

Once of the sRGB values were calculated a color plot was created showing the color of the spectrum at each sample location about the crystal. Figure 54 is the resulting color plot. The x-axis shows the response as theta is varied, and the y-axis shows the response as phi is varied. It can be seen that the color changes from orange to blue as theta is varied. The black corresponds to low intensity of the crystal response. The plot also shows that when the crystal is rotated to 45 degrees there is again a crystal response that shifts out of the measurement window was theta is decreased.

Summary

The custom test stand that was designed and built provides a flexible system for interrogating the out-of-plane emissions from 2D photonic crystals. This stand enables the spectrum of the emission response to be sampled at a fixed distance surrounding the crystal. The custom test stand design makes use of an old XRD stand and modifies it for the purpose of the experiment. The unmodified XRD stand allows for the rotation of the crystal on multiple axes while keeping the crystal fixed at the center of the system. This rotation of the crystal simulates some of the movements of the collection point around the crystal required for the experiment. The rest of the required movements are accomplished with a rotation arm that was added to the stand. The light source and detection points of the system are collinear by using a reflection probe that is made up of multiple optical fibers.

The use of the stand was then demonstrated, and the measured spectra of the emission response were analyzed and used to create a color plot. It was found that the light source and coloration from the substrate that the photonic crystal is built on affected the spectra of the crystal's response. These effects were removed during the analysis. The spectra were then weighted by a color matching function and converted to sRGB values for use in creating the color plot. The purpose of the color plot is to allow for a quick visual synopsis of the crystal response at each sample location. Points of interest can then be further investigated by then looking directly at the spectra of the crystal

response at those points. The resulting plot shows the color variation as the sampling location is varied and successfully demonstrates the stand's use.

Works Cited

[1] S. McBeath, "LightGauge: Production of Photonic Sensor on Nuclear Materials," Idaho State University, Pocatello, 2014.

[2] International Atomic Energy Agency, "Modern Instrumentation and Control for Nuclear Power Plants: A Guide Book," IAEA, Austria, 1999.

[3] J. D. Joannopoulos, S. G. Johnson, J. N. Winn and R. D. Meade, Photonic Crystals: Molding the Flow of Light, New Jersey: Princeton University Press, 2008.

[4] S. Reyntjens and R. Puers, "A review of focused ion beam applications in microsystem technology," *Journal of Micromechanics and Microengineering,* vol. 11, no. 4, pp. 287-300, 2001.

[5] S. McBeath, Artist, *Graduate Student Researcher.* [Art]. Idaho State University RISE, 2014.

[6] C. W. Neff, "Optical Properties of Superlattice Photonic Crystals," Georgia Tech University, Atlanta, 2005.

[7] J. D. Joannopoulus, "The Almost-Magical World of Photonic Crystals," *Brazilian Journal of Physics,* vol. 26, no. 1, pp. 58-67, 1996.

[8] E. Burgett, "Novel Neutron Detectors," Georgia Tech University, Atlanta, 2010.

[9] T. Hill, Interviewee, *Dr..* [Interview]. May 2014.

[10] R. A. Serway and J. W. Jewett, Physics for scientists and engineers, Belmont: BROOKS/COLE CENGAGE Learning, 2008.

[11] "Technai Basic Procedure," [Online]. Available: http://web.stanford.edu/group/snl/old/TEM/Tecnai%20Basic%20Procedures.pdf. [Accessed 17 Nov 2014].

[12] Lambda Scientific, "LEOI-100 Experimental CCD Spectrometer User's Manual," Miami.

[13] "National Institute of Standards and Technology," U.S. Department of Commerce, 2013. [Online]. Available: http://www.nist.gov/pml/data/asd.cfm. [Accessed 13 Aug 2014].

[14] G. Wyszecki and W. S. Stiles, Color Science: Concepts and Methods, Quantitative Data and Formulae, New York: Wiley, 2000.

[15] R. W. G. Hunt and M. R. Pointer, Measuring Colour, Chichester, West Sussex: Wiley, 2011.

[16] International Color Consortium, "Specification of sRGB," [Online]. Available: http://www.color.org/chardata/rgb/sRGB.pdf. [Accessed 13 Nov 2014].